

# Journal Pre-proof

Thermo-mechanical performance of nanostructured electrospun composites produced from poly(vinyl alcohol) and cellulosic compounds for potential uses as wound dressings

Marta A. Teixeira, Aureliano Fertuzinhos, David S. Freitas, Carla Silva, Diana P. Ferreira, Helena P. Felgueiras

PII: S0032-3861(23)00461-5

DOI: <https://doi.org/10.1016/j.polymer.2023.126131>

Reference: JPOL 126131

To appear in: *Polymer*

Received Date: 18 January 2023

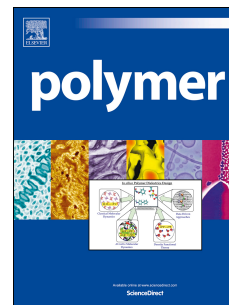
Revised Date: 26 May 2023

Accepted Date: 19 June 2023

Please cite this article as: Teixeira MA, Fertuzinhos A, Freitas DS, Silva C, Ferreira DP, Felgueiras HP, Thermo-mechanical performance of nanostructured electrospun composites produced from poly(vinyl alcohol) and cellulosic compounds for potential uses as wound dressings, *Polymer* (2023), doi: <https://doi.org/10.1016/j.polymer.2023.126131>.

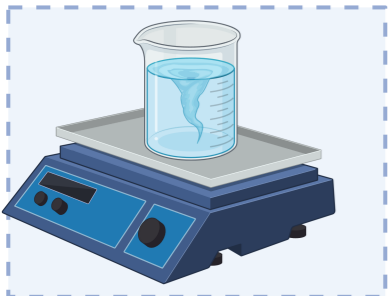
This is a PDF file of an article that has undergone enhancements after acceptance, such as the addition of a cover page and metadata, and formatting for readability, but it is not yet the definitive version of record. This version will undergo additional copyediting, typesetting and review before it is published in its final form, but we are providing this version to give early visibility of the article. Please note that, during the production process, errors may be discovered which could affect the content, and all legal disclaimers that apply to the journal pertain.

© 2023 Published by Elsevier Ltd.

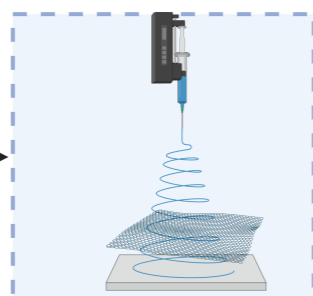


Investigation, M.A.T., A.F.; Data curation, M.A.T.; Writing - original draft preparation, M.A.T.; Writing - review and editing, A.F., D.S.F., C.S., D.P.F., H.P.F.; Supervision, D.P.F., H.P.F.; Funding acquisition, H.P.F. All authors have read and agreed to the published version of the manuscript.

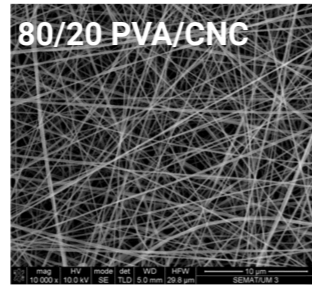
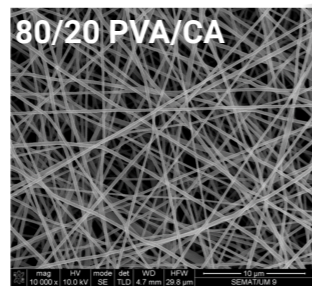
Journal Pre-proof



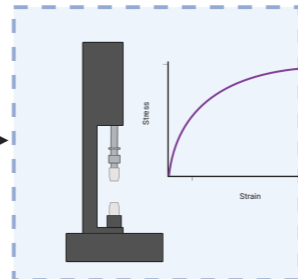
1 Preparation of solutions (PVA/CA and PVA/CNC)



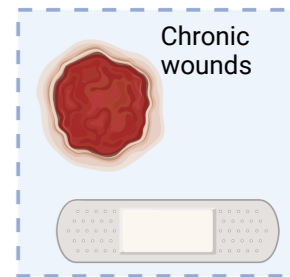
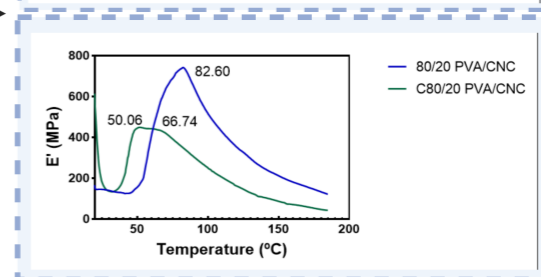
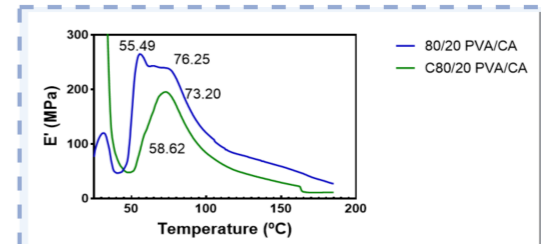
2 Electrospinning



3a Characterization (analysis by SEM; XRD, TGA, DSC)



3b Mechanical Testing: Uniaxial and DMA tests



Chronic wounds

## Thermo-mechanical performance of nanostructured electrospun composites produced from poly(vinyl alcohol) and cellulosic compounds for potential uses as wound dressings

Marta A. Teixeira<sup>1</sup>, Aureliano Fertuzinhos<sup>2</sup>, David S. Freitas<sup>3</sup>, Carla Silva<sup>3</sup>, Diana P. Ferreira<sup>1</sup>, Helena P. Felgueiras<sup>1,\*</sup>

<sup>1</sup>Centre for Textile Science and Technology (2C2T), Department of Textile Engineering, University of Minho, Campus of Azurém, 4800-058 Guimarães, Portugal

<sup>2</sup>Center for MicroElectroMechanics Systems (CMEMS), Department of Mechanical Engineering, University of Minho, Campus of Azurém, 4800-058 Guimarães, Portugal

<sup>3</sup>Centre of Biological Engineering, University of Minho, Campus de Gualtar, 4710-057 Braga, Portugal

**ABSTRACT.** The purpose of this research was to analyze the morphology, thermal and mechanical properties of poly(vinyl alcohol) (PVA)-based electrospun mats reinforced with cellulose acetate (CA) or cellulose nanocrystalline (CNC) for potential applications in wound dressings. Bead-free and water-stable electrospun nanofibers made of blends of PVA and CA or CNC were successfully produced and crosslinked with glutaraldehyde vapor. Crosslinking slightly increased the nanofibers' diameters in order of 43 and 13% for 80/20 PVA/CA and PVA/CNC electrospun mats, respectively, while maintaining their bead-free morphology. Thermogravimetry (TGA) and differential scanning calorimetry (DSC) evaluations were employed to determine the miscibility and the thermal response of the uncrosslinked and crosslinked mats, reporting a reduction in mass loss upon addition of CA and CNC and upon crosslinking process. Polymers' powder and mats (before and after crosslinking) crystallinity was assessed by X-ray diffraction analysis (XRD). Crosslinked mats experienced a slight reduction in crystallinity compared to the uncrosslinked. Static and dynamic tensile strength tests revealed that CA and CNC doped mats enhanced the Young's modulus and lowered deformation at failure compared to pristine PVA electrospun mats. Data from storage modulus ( $E'$ ) demonstrated the strength of the physical interactions formed between PVA and the cellulosic derivatives (either before and after crosslinking), highlighting the stiffness of CA (231.58 MPa for the 80/20 mat) and, particularly, CNC (742.04 MPa for the 80/20 mat). This research uncovered important information concerning the chemical and physical relation between polymeric matrices and additives, essential for the proper selection of materials for wound dressings production.

**KEYWORDS.** Poly(vinyl alcohol); cellulose acetate; cellulose nanocrystalline; thermal behavior; quasi-static and dynamic mechanical performances.

### 1. INTRODUCTION

Skin wounds are an important healthcare and social problem worldwide, being associated with high morbidity and mortality rates [1,2]. New generation of wound dressings have been engineered and used to assist in promoting and accelerating skin regeneration, while protecting the wounded site from further harm [3,4]. In the last decades, bandages and gauzes have been the dressings of choice for accelerating scar formation, despite their inefficiency in protecting the wound against infection and their replacement at the injured site being responsible, in many instances, for causing pain and removing newly formed cell tissue [5]. Therefore, research for new dressing alternatives has become essential.

During the development of a modern wound dressing, specific requirements must be taken into consideration, namely non-immunogenicity, non-toxicity, ability to absorb wound exudates, proper breathability, protection against microbial infection, biodegradability, and suitable mechanical properties for an effective adaptation to the wounded site [2,6–9]. Modern wound dressings can be

constructed in the form of films, hydrogels, hydrocolloids, 3D scaffolding systems, and nanofibrous mats [10,11]. The last have been highlighted for their outstanding physiochemical properties and extraordinary biological performance [12,13]. Indeed, nanofibrous mats' large specific surface area, high porosity, small pore size, and excellent channel connectivity have shown to promote wound hemostasis (absorb necrotic tissue and exudates), protect against bacterial penetration (nanoscale barrier with pore size smaller than bacteria), and generally instigating healing (facilitate the oxygenation of cell tissues, preventing drying and dehydration) [14–19]. Additionally, the large specific surface area that characterize these systems facilitates loading of molecules of interest, including antimicrobial and regenerative drugs. The intertwined and connected structure of the non-woven nanofibers can mimic the structure and biological functions of the extracellular matrix (ECM), providing a good template for cell adhesion, proliferation, and growth, aside from being more easily recognized by the human body for a quicker integration [19,20].

Even though many techniques can be used for generating nano-scaled systems for wound healing, electrospinning can be highlighted for its simplicity, inexpensive and scalable production, and facility of processing of both synthetic and natural polymers [21,22]. Biomedicine has mostly focused on synthetic biodegradable polymers such as polycaprolactone (PCL), poly(lactic acid) (PLA), poly(L-lactide) (PLLA), poly(lactic-co-glycolic acid) (PLGA), and polyvinyl alcohol (PVA), due to their ease of processing, abundance, and superior mechanical strength compared to the natural-origin options [23–25]. PVA, a highly water-soluble polymer approved by the USA Food and Drug Administration (FDA), is an ideal candidate for nanofibrous dressing production because of its non-toxic nature, chemical resistance, biocompatibility, and biodegradability [6,26–28]. Yet, PVA-based electrospun nanofibers have been described as insufficiently strong to endure specific uses, considering PVA behaves as a soft material with relatively high strain and low stiffness [29,30]. To improve such features, many approaches have been proposed, including post-treatments (heat treatment, hot pressing, stretching, hot stretching, solvent welding, etc.) [31–33], alteration of fiber orientation via different collectors and electric field applications (aligned) [34], crosslinking (physical, chemical) [35], and blending with other materials [36]. Introduction of nanomaterials into PVA matrices has been most effective in reinforcing electrospun PVA nanofibers [37–42]. In recent years, incorporation of cellulosic materials, in the form of fibers, particles and whiskers, into electrospun nanofibrous mats has paved the way for engineering new fiber nanocomposites. These renewable, highly abundant, and low-cost cellulosic additives can establish reliable and durable bonds with PVA, improving the composite mechanical and physical properties above the pristine polymer [43–45]. On its own, cellulose presents limited solubility in general organic solvents and cannot be melt due to its large amount of inter- and intra-molecular hydrogen bonds, hindering its biomedical applications [46,47]. To overcome these drawbacks various chemical derivatives of cellulose and different nanocelluloses have been investigated. Cellulose acetate (CA) is perhaps the most researched cellulose derivative, being frequently found in wound dressing formulations [48,49]. CA displays outstanding properties of biodegradability, biocompatibility, hydrolytic stability, insolubility in water, non-toxicity, and good mechanical strength [50]. Because of the hydroxyl groups available in CA, chemical bonding with PVA is easily achieved [51,52]. Among the nanocelluloses, nanocrystalline cellulose (CNC) has gained enormous interest for incorporation into polymeric matrices because of its excellent dispersion, particularly in water, and large amount of surface free hydroxyl groups. CNCs are suitable nanofillers for reinforcing PVA matrices by generating strong interactions via hydrogen bonding at the interface between CNC and PVA [53,54]. Furthermore, CNCs are “green” compounds (low environmental impact), biocompatible, biodegradable, have a high aspect ratio, and a high Young's modulus, conferring exceptional physical and mechanical features to the nanofibrous mats. They may also facilitate the electrospinnability of polymer blends via their high surface charge, a result of the acid hydrolysis they are subjected to, which improves nanofiber alignment and consequently the mats' mechanical performance [55,56].

Many studies have investigated the impact of incorporating CA or CNC into PVA-based electrospun mats for wound healing applications [27,55,57,58]. Here, the scientific community tends to focus on biological issues or, when investigating the physical and mechanical properties of designed substrates, does not go beyond the normal fracture analysis of reinforced polymeric matrices. Yet, it is well established that the mechanical properties of wound dressing materials also affect cellular activities, reporting a high dependency of the cell matter interplays to the applied shear stresses and mechanical signaling channels that control the migration, proliferation, and differentiation of cells [59].

Our research investigates the mechanical properties of PVA/CA and PVA/CNC electrospun mats, before and after chemical crosslinking, and supplements those analyses with morphological and thermal evaluations to provide a comprehensive understanding of the performance of the engineered electrospun nanofibrous mats.

## 2. MATERIALS AND METHODS

**2.1 Materials.** PVA (partially hydrolyzed, 88% with medium Mw (molecular weight), 78,000) was purchased from Polysciences, Europe GmbH. CA (39.8 wt.% acetyl content, Mw 30,000) was acquired from Sigma (Taufkirchen, Germany), and CNC with diameters of approximately 75 nm and polydispersity index (PDI) of 0.181 was purchased from CelluForce (Montreal, Canada). The acetic acid (glacial) was obtained from Merck (Darmstadt, Germany) and the glutaraldehyde (GA, 25% aqueous solution) from Sigma (Taufkirchen, Germany). All reagents were used without further purification.

**2.2 Production of nanofibrous mats.** Polymeric solutions of PVA/CA and PVA/CNC were prepared at 10% (w/v) at varying ratios: 100/0 (or 100 PVA), 90/10 and 80/20% (v/v). Solutions with polymeric ratios with increased amounts of CA and CNC could not be successfully produced. PVA/CA solutions were prepared in acetic acid/distilled water (dH<sub>2</sub>O) at 75/25% (v/v), being continuously stirred for 4 h at 40 °C. PVA/CNC solutions were prepared separately in dH<sub>2</sub>O, being PVA dissolved at 40 °C and CNC at room temperature, both for 4 h. PVA and CNC solutions were then mixed and left under continuous stirring for 2 h at room temperature. To ensure CNC dispersion, the mixture was subjected to sonication bath for 2 h. After, to determine the viscosity of the polymeric solutions, a viscometer Brookfield DV – II+ Pro with a 27 and 21 spindle, respectively for PVA/CA and PVA/CNC, and a speed of 50 rpm at 40 °C was used, performing data readings in intervals of 30 s for a period of 4 h (duration established for electrospun fiber deposition). The conductivity and zeta-potential (mV) of the blends were measured using a Zetasizer Nano ZS (Malvern Instruments) at room temperature.

Regarding the electrospinning, the processing conditions were optimized to a voltage of 25 kV applied to a steel capillary needle with an inner diameter of 18 Gauge (G), attached to a 5 mL syringe containing the prepared solutions. The flow rate was established at 0.8 mL/h. Aluminum sheets were used as nanofiber collectors (ground) and were placed at a vertical distance of 180 mm. Temperature and relative humidity (RH) were controlled and maintained at 20-22 °C and 65-70%, respectively. The produced electrospun nanofibers were stored in a desiccator with a controlled RH of approximately 41% at room temperature.

**2.3 Crosslinking.** PVA/CA and PVA/CNC mats were crosslinked in GA vapor to increase their stability in aqueous media. Mats of 130×120 mm<sup>2</sup> were first dried overnight at 40 °C, to eliminate residual water molecules, and then placed in a vacuum-sealed desiccator with 6 mL of GA solution, during 7 h at 60 °C. In the end, mats were stored in a controlled environment of 41% RH and room temperature to allow any residual GA to be eliminated over time. For proper identification, the uncrosslinked mats were labelled as 100/0, 90/10 and 80/20, while the crosslinked mats were named as C100/0, C90/10, and C80/20.

**2.4 Field emission gun scanning electron microscopy (FEG-SEM).** Morphological analyses of the mats' surface were conducted via FEG-SEM (NOVA 200 Nano SEM, FEI Company) with an accelerating voltage of 10 kV. Mats were initially coated with a thin layer (10 nm) of gold-palladium (Au-Pd, 80-20 wt.%), using a 208HR high-resolution sputter coater (Cressington Company, Watford WD19 4BX, United Kingdom) coupled to an MTM-20 Cressington High Resolution Thickness Controller. The average diameters of the uncrosslinked and crosslinked electrospun mats were determined by conducting 100 measurements of nanofibers diameters from three micrographs of each PVA/CA and PVA/CNC ratio (100/0, 90/10 and 80/20% v/v). Images at a magnification of 50,000 $\times$  were used and processed using the ImageJ software, to obtain the diameter distribution with a log-normal function. The number of layers and porosity of the mats were also evaluated from four micrographs collected from each polymer ratio of both combinations resorting to the Python software. Details of porosity determinations are provided in Section S1 of the Supporting Information file. All nanofiber mats' diameters and porosities were presented as mean  $\pm$  standard deviation (S.D.).

**2.5 X-ray diffraction (XRD) studies.** XRD measurements were performed to determine the crystallinity of the PVA/CA and PVA/CNC electrospun mats and PVA, CA and CNC powders using AXS D8 Discover-Bruker diffractometer operating with a Cu K $\alpha$  radiation source ( $\lambda=1,54060\text{\AA}$ ), generated at 40 kV and 40 mA. XRD spectra were recorded in the  $2\theta$  angle, using a scale ranging from 5 to 50 $^\circ$  at a rate of 0.04 $^\circ$ /s.

**2.6 Thermal analysis.** Thermal gravimetric analysis (TGA) and differential scanning calorimetry (DSC) were performed to evaluate the structural and thermal stability and phase transitions of the produced mats by means of weight loss, glass transition and melting temperatures. TGA were carry out between 25 and 600  $^\circ\text{C}$ , at a heating rate of 10  $^\circ\text{C}/\text{min}$  under a dynamic nitrogen atmosphere and flow rate of 200 mL/min (inert environment), on a STA 7200 Hitachi $^\circ$  (Fukuoka, Japan) using aluminum pans. The initial mass of each sample was established at  $5 \pm 2$  mg. Results were plotted as percentage of weight loss vs temperature. Derived thermogravimetric (DTG) spectra were also acquired, to identify temperature ranges where degradation was most significant.

DSC data were obtained using a DSC 822 Mettler Toledo (Columbus, USA). Samples of  $5 \pm 2$  mg were sealed in an aluminum pan and subjected to a first heating step (0-100  $^\circ\text{C}$ , to remove absorbed and adsorbed water), followed by cooling, and then to a second heating step (0-250  $^\circ\text{C}$ ) at a rate of 10  $^\circ\text{C}/\text{min}$ , under a dynamic nitrogen atmosphere, and flow rate of 20 mL/min (inert environment). The glass-transition temperatures ( $T_g$ ), melting temperatures ( $T_m$ ) and enthalpies ( $\Delta H$ ) were established.

**2.7 Uniaxial tensile tests.** The tensile strain of the electrospun mats was measured using the uniaxial tensile test. Samples were prepared following ASTM D5035-11 (2019). The gauge length was set to 30 mm. Hounsfield Universal Testing Machine (Hounsfield UTM) with a 250 N loading cell was used to run the tensile test at displacement rate of 3.0 mm/min and room temperature. Prior to testing, a low tare load was applied to establish a consistent zero position. Young's modulus (MPa), ultimate tensile strength (UTS, in MPa) and strain at failure (%) were obtained from stress-strain curves. Measurements were conducted in triplicate.

**2.8 Dynamic mechanical analysis (DMA).** DMA was performed using a DMA 7100 from Hitachi $^\circ$  (Fukuoka, Japan) in programmed tension (viscoelastic behavior) using the operating software of the equipment. Strips of  $20 \times 5$  mm $^2$  with an average thickness of  $0.75 \pm 0.2$  nm were cut from the nanofibrous mats for DMA testing. The storage modulus ( $E'$ ) was determined in the temperature range of 20 to 250  $^\circ\text{C}$  at 3  $^\circ\text{C}/\text{min}$  using a single frequency (1 Hz) in synthetic oscillation. The glass transition temperature ( $T_g$ ) of the electrospun mats was identified through the onset of  $E'$  drop. This DMA method has revealed great precision in determining the  $T_g$  of a variety of viscoelastic polymer-based

materials [60]. Examinations were carried out in a nitrogen atmosphere at 200 mL/min, to ensure an inert environment. Measurements were conducted in triplicate.

### 3. RESULTS AND DISCUSSION

PVA selected was chosen because of its excellent solubility in water, even at low temperatures, and for presenting a lower surface tension, compared with the highly hydrolyzed PVA, enabling electrospinning [61,62]. Additionally, the PVA used is mechanically more resilient than the highly hydrolyzed version of the polymer [6]. To guarantee the formation of a uniform and stable polymer jet during electrospinning, 10% w/v was established as the ideal working polymer concentration. The solution concentration affects the polymer chains entanglement and the formation of a continuous physical network [63].

Both PVA/CA and PVA/CNC electrospun mats were water-unstable after production, progressively dissolving; thus, requiring an efficient crosslinking to form a three-dimensional water-resistant network. For this purpose, chemical crosslinking with GA vapor was employed. GA is a crosslinker widely used in PVA treatments due to its low cost, facile processing, and great efficiency [64]. However, GA has been recognized as cytotoxic, with consequences being dependent upon the concentration used and the type of cells tested [65,66]. Yet, the GA vapor phase methodology has been described as an approach with low or no detectable cytotoxic effects [7,67,68]. Chemical crosslinking entails the formation of covalent bonds between different molecular chains. Here, the crosslinking reaction was established via acetal bridges between the difunctional aldehyde of GA and the hydroxyl groups of the polymers [69–71]. To minimize nanofiber softening, swelling and retention of water molecules arising from the GA solution (composed of 75% of water), and considering the water vapor pressure is higher than GA vapor pressure [72], a sealed vessel with silica was used during crosslinking. Here, 6 mL solution of 2.56 M GA heated to 60 °C for 7 h, to generate vapor, was applied to all samples. These conditions were deemed effective in achieving nanofibers' crosslinking. This methodology, compared with other literature reports, appeared to be less severe, since it did not require an acidic catalyst [73,74], long vacuum periods [75,76] or temperatures in the order of 100 °C [77], either during crosslinking or for GA removal after crosslinking.

**3.1 Characterization of the spinning solution and the nanofiber's morphology.** Micrographs of electrospun PVA/CA and PVA/CNC nanofibers were collected (Figure 1). All fibers produced were in the nanoscale range and no beads or bead-on-string structures were visible. Nanofibers electrospun from PVA/CA solutions displayed the largest diameters and widest diameter distribution.  $223 \pm 50$ ,  $217 \pm 73$  and  $194 \pm 51$  nm were the average diameters achieved for the 100/0, 90/10 and 80/20 PVA/CA nanofibers, respectively, while for 100/0, 90/10 and 80/20 PVA/CNC they were in the order of  $172 \pm 40$ ,  $171 \pm 38$  and  $132 \pm 26$  nm (Table 1). Nanofibers size diameters and morphology are conditioned by the viscosity, conductivity of the polymeric solutions and specific solvent properties, such as boiling point (b.p.) and dielectric constant ( $\epsilon$ ) [78–80]. For this reason, polymeric solutions were characterized regarding viscosity, conductivity, and zeta potential (Table 1). All PVA/CA solutions (100/0, 90/10 and 80/20) prepared with 75/25% v/v of acetic acid/dH<sub>2</sub>O presented a higher viscosity than the PVA/CNC blends prepared only with water, which explains the larger diameters detected [1,6,44,81]. Additionally, by looking at the neat PVA solutions (100/0 PVA/CA and PVA/CNC), the contribution of the solvents to the parameters listed in Table 1 becomes even clearer. Mahmud et al., on studying solvent systems, established that the acetic acid/dH<sub>2</sub>O combination increases polymeric solutions' viscosity over systems prepared with 100% dH<sub>2</sub>O and showed a tendency of decreasing conductivity with higher amounts of acetic acid [82]. These conclusions are in concordance with our results. It is also worth noting the importance of the b.p. and the  $\epsilon$  of the solvents employed. dH<sub>2</sub>O and acetic acid have b.p. of 100 and 118 °C and  $\epsilon$  of 79.7 and 6.2 at 20 °C, respectively [80,83,84]. The boiling point of acetic acid is 118 °C, higher than that of dH<sub>2</sub>O, which may explain the increase in fiber diameter registered and the longer time required for evaporating the solvent. As  $\epsilon$



indicates the ability of a material to become electrically polarized and store electrical energy [80], it could also explain the smaller size diameters of the formulations PVA/CNC (namely the 100/0 ratio). As dH<sub>2</sub>O polarizes faster than acetic acid (due to its higher  $\epsilon$ ) under an electric field similar to the one applied during electrospinning, a greater interaction between polymer and solvent (instead of polymer-polymer) is expected, thus interfering with the conformation of the polymeric chains in the solution and, consequently, with the viscosity and the resulting fiber diameters [79,80,85]. Solvent systems with high dielectric constants tend to instigate the formation of electrostatic fields. Hence, it would not be surprising if the electrostatic field strength required for a stable jet formation increased with the increasing  $\epsilon$  value of the solvent system [75,80]. In the present study, and for comparison purposes, similar voltage fields were used for both PVA/CA and PVA/CNC. The addition of CA and CNC to the PVA solution decreased the mixture viscosities (Table 1), which may result from a reduction on the entanglement of the PVA chains. It was also seen that the addition of CNC increased the conductivity of the solution, which is attributed to the high surface charge of the CNC acquired by the formation of sulfate ester groups after hydrolysis with sulfuric acid [29,86]. The presence of these negatively charged groups on the polymeric blend was verified by zeta potential evaluation (Table 1) and raised as the content in CNCs increased. These charges contributed to the production of more homogeneous and smaller diameter nanofibers, as they increased the electrical force imposed on the polymer jet [87]. Because of the alterations CA and CNC introduced on the viscosities and conductivities, the nanofiber diameters were found smaller than those obtained with neat PVA; the 80/20 PVA/CNC reached the smallest diameters from the tested samples. After crosslinking, the morphological features of the nanofibers did not alter, but the diameters in general increased in response to the interaction between the aldehyde groups of GA and the hydroxyl groups of the polymers [88]. The only exception was observed on C100/0 PVA/CA nanofibers, which showed a reduction in diameter after crosslinking, contrarily to the predictions described previously. The decrease in diameters might be attributed to the lower amount of GA linked to this mat as a result of increased hydrogen bonds between PVA chains, and, possibly, to the presence of acetic acid, which has a higher boiling point (118 °C) than water (100 °C) [89]. Acetic acid can interfere with the formation of acetal linkages between the hidroxil groups of PVA and the aldehyde groups of GA. It does not imply that the electrospun mats displayed dimensional instability (a1), but it may have a lower GA quantity on the surface of the nanofibers than others, contributing to the verified smaller diameters. CA-containing nanofibers were more affected than the CNC-containing nanofibers particularly the 80/20 combination, which increased in  $\approx$  43% the average fiber diameter compared to the  $\approx$  13% increment verified for the same polymer ratio of PVA/CNC. This could be related with the positioning and distribution of the reinforcing agents since CA can be entangled with PVA throughout the chain's length with great interconnection and freedom of movement, while the CNC being more compact (because of its crystallinity) could be distributed along these chains with a more restricted number of interactions and thus a smaller contribution to the dimension of the fibers. The mats porosities did not register an important alteration (Table 1), being considered effective for the foreseen application. High porosities (around 60 to 90%) are regard as suitable for appropriate local moisture and good oxygenation of wound beds, by stimulating cell proliferation [6,90,91]. However, they may also allow bacteria infiltration [92]; therefore, moderate porosities are desired [93,94]. However, the lower porosity values obtained may be related with the mats' thickness, relatively high density, and structural rigidity of electrospun mats produced [26,95] Despite that, they may be considered suitable alternatives for the treatment of chronic dry wounds and in scar prevention, or to be used as supplemental structures in other dressings to reach an appropriate balance on this parameter [96].

**Table 1.** Polymeric blends properties and subsequent electrospun mats' fiber diameters and porosities, before and after chemical crosslinking with GA vapor. Data is reported as mean  $\pm$  SD. Statistical significance between nanofiber diameters was determined via Kruskal-Wallis test applying multiple comparisons between uncrosslinked and crosslinked electrospun mats. Most comparisons were deemed significant with  $p < 0.0001$ ; exceptions were seen for 100/0 vs 90/10, 100/0 vs. C90/10, 90/10 vs. C90/10 and 80/20 vs C100 for PVA/CA, and 100/0 vs 90/10 and 90/10 vs C90/10 for PVA/CNC, which did not report significant differences. The comparison 90/10 vs. C100 PVA/CA reported a  $p < 0.0007$  significance.

	Polymer ratios	Viscosity (cP)	Conductivity ( $\mu$ S/cm)	Zeta potential (mV)	Diameter before crosslinking (nm)	Diameter after crosslinking (nm)	Porosity before crosslinking (%)	Porosity after crosslinking (%)
PVA/CA	<b>100/0</b>	2360 $\pm$ 70.12	328 $\pm$ 12.11	0.042 $\pm$ 0.11	223 $\pm$ 50.01	200 $\pm$ 60.00	20 $\pm$ 5.12	18 $\pm$ 2.68
	<b>90/10</b>	2365 $\pm$ 41.02	282 $\pm$ 15.17	0.024 $\pm$ 0.02	217 $\pm$ 73.02	238 $\pm$ 93.01	28 $\pm$ 5.48	16 $\pm$ 5.22
	<b>80/20</b>	1450 $\pm$ 11.10	229 $\pm$ 11	0.074 $\pm$ 0.10	194 $\pm$ 51.12	278 $\pm$ 56.03	19 $\pm$ 3.49	15 $\pm$ 3.57
PVA/CNC	<b>100/0</b>	495 $\pm$ 4.79	718 $\pm$ 8.00	0.100 $\pm$ 0.10	172 $\pm$ 40.13	220 $\pm$ 50.13	18 $\pm$ 0.44	19 $\pm$ 5.59
	<b>90/10</b>	467 $\pm$ 10.01	724 $\pm$ 7.00	1.570 $\pm$ 0.21	171 $\pm$ 38.21	180 $\pm$ 37.11	20 $\pm$ 0.93	19 $\pm$ 0.41
	<b>80/20</b>	394 $\pm$ 10.11	880 $\pm$ 4.21	2.250 $\pm$ 0.19	132 $\pm$ 26.01	150 $\pm$ 30.23	24 $\pm$ 3.12	22 $\pm$ 1.35

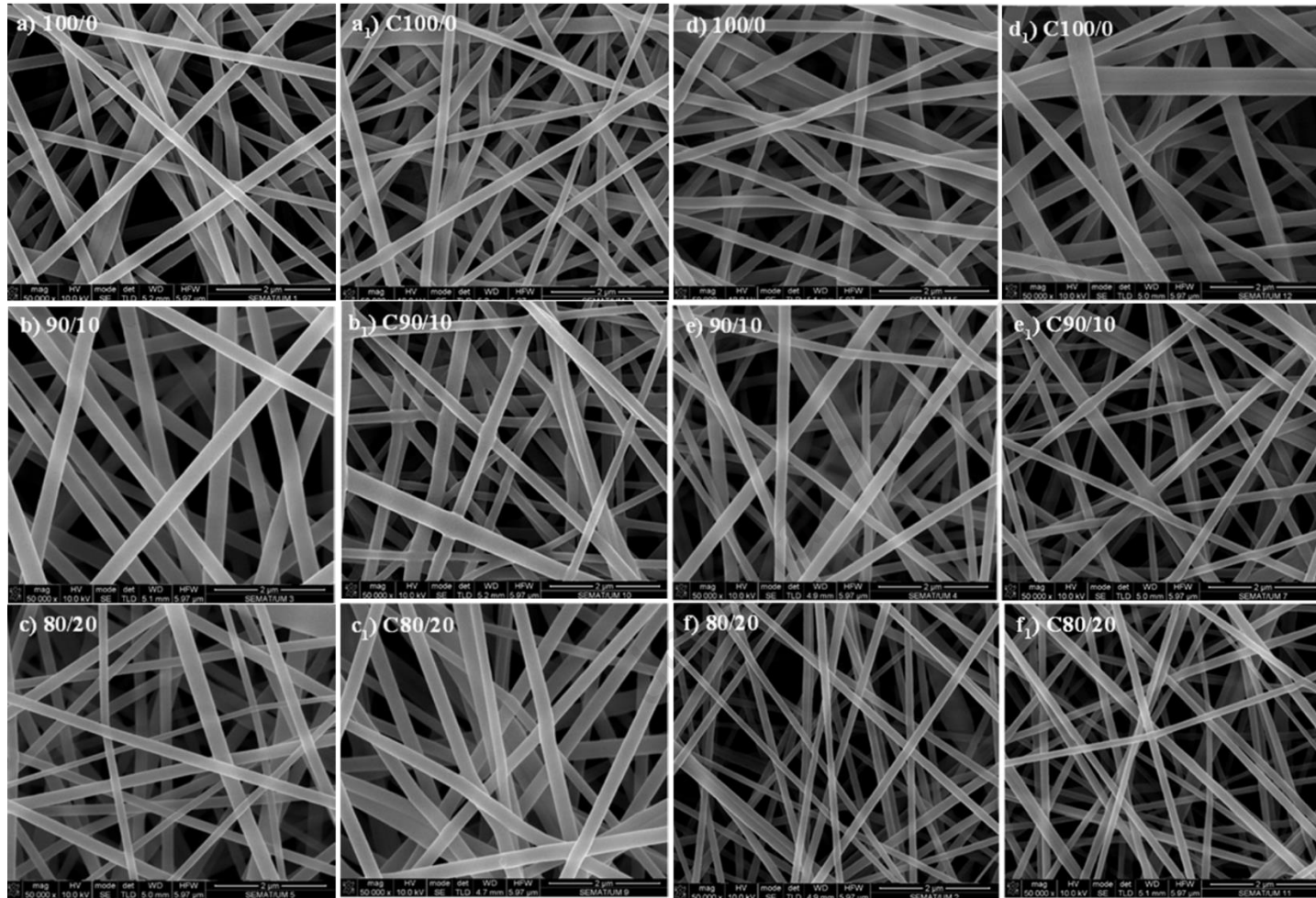


**Figure 1:** FEG-SEM micrographs of 100/0, 90/10 and 80/20 PVA/CA and 100/0, 90/10 and 80/20 PVA/CNC mats, before crosslinking (a, b, c, d, e, and f, respectively) and after crosslinking (a<sub>1</sub>, b<sub>1</sub>, c<sub>1</sub>, d<sub>1</sub>, e<sub>1</sub> and f<sub>1</sub>, respectively). Scale bar of 2 μm.

**3.2 X-ray diffraction studies.** XRD analyses were used to determine the crystallinity of the electrospun mats and of the polymer powders and to understand the influence of the crosslinking process on that property (Figure 2). This non-destructive analytical technique is frequently used for crystalline phase identification and provides information regarding crystallographic structure, chemical composition, and physical properties of materials [97].

XRD diffractogram of PVA powder detected two characteristic peaks at  $19.6^\circ$  and  $22.8^\circ$ , which were attributed to the 101 and 002 crystal planes, respectively [98,99]. Furthermore, a diffraction peak was also observed at  $40.6^\circ$ , indicating PVA to be a semi-crystalline polymer, which crystallinity originates from strong intermolecular interactions between its chains [100,101]. However, after electrospinning, PVA mats revealed an amorphous nature with the significant attenuation of the polymer most salient peak at  $2\theta = 19.6^\circ$  and the complete absence of the peak at  $2\theta = 41.1^\circ$  (Table 2). It was evident that the crystallinity of the polymers was diminished after electrospinning, a phenomenon verified also by other authors [102]. Here, the PVA powder's crystallinity was determined at  $\approx 30.5\%$ , while the 100/0 PVA/CA and 100/0 PVA/CNC presented a degree of crystallinity of 26.1 and 23.0%, respectively.

Mats' crystallinity increased with the addition of 10% CA; yet the addition of 20% CA had the opposite effect (Table 2). Data suggests that there is a limit up until which PVA and additives can organize themselves to guarantee a crystalline arrangement but, once surpassed, structural disorganization and consequently lower crystallinities are attained. This could indicate that the introduction of additives at concentrations superior to those permissible by the matrix polymer, in which crystalline organization is still possible, can perturb the packing of the PVA chains [45,103–105]. On its turn, introduction of higher amounts of CNC in the polymeric blend led to an increase of crystallinity, rising from 23.9% for 100/0 PVA/CNC to 25.1 and 30.8% for 90/10 and 80/20 PVA/CNC electrospun mats, respectively. These data confirm the densely and orderly stacking structure obtained with this mixture, a result that can be attributed to the inherent crystallinity of the CNC and their uniform distribution along the nanofibers, guiding molecular orientation [45]. Generally, evidence of the excellent miscibility between polymers was acquired [45,103,106].

On the CA powder XRD diffractogram, a broad peak in the region of  $2\theta = 10\text{--}30^\circ$  was detected. It has been described as the characteristic peak of the amorphous CA parts [97,107]. This was not seen in any of the PVA/CA electrospun mats XRD diffractograms, considering its low influence on the crystallinity of the blend (PVA powder had a superior contribution). However, interestingly, the peak detected at  $23.3^\circ$  for CNC powder was evidenced on all CNC-containing mats. It was more intense on 80/20 PVA/CNC mats, reinforcing the premise of the optimal crystalline arrangement and optimal blending ratio with PVA matrices. It also corroborates the affinity between the polymers and the higher crystallinity of CNC. Indeed, three well defined peaks were identified on the CNC XRD diffractogram at  $2\theta = 16.1^\circ$ ,  $23.3^\circ$ , and  $35.2^\circ$  on the (1 1 0), (2 0 0) and (0 0 4) planes, respectively, which are associated to the characteristic peaks of  $I_\beta$  [108–110].

After crosslinking, mats experienced a small reduction in crystallinity (Figure 2 and Table 2). Li et al. also observed the same effect [111]. They explained that on uncrosslinked PVA mats intermolecular hydrogen bonds are generated between PVA chains, which are beneficial to the directional alignment of the chains and, consequently, to the organization of the crystalline phase of the polymer. On crosslinked mats a smaller number of hydrogen bonds are formed and, therefore, the polymer exhibits less crystallinity. From the morphological analyses (Figure 1 and Table 1), it was also evidenced that the acetal bonds affected the polymers' structural organization, thus supporting such outcomes.

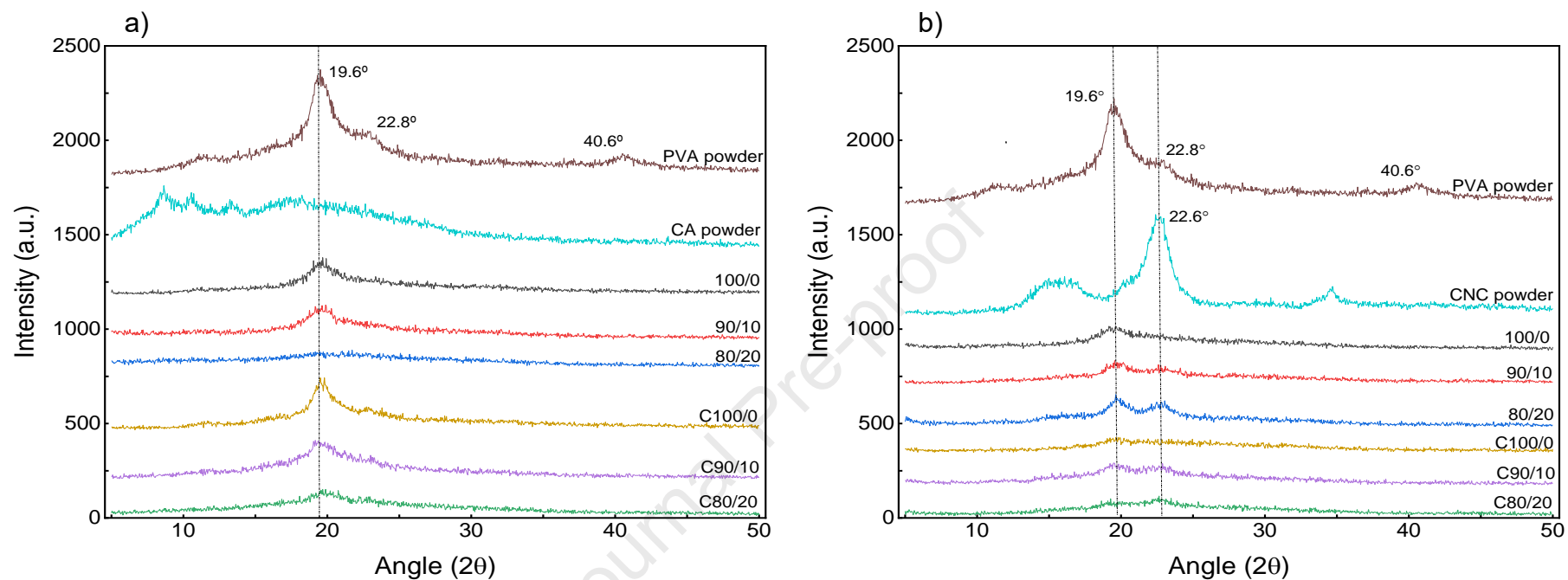


**Figure 2:** XRD patterns of a) PVA, CA powders and uncrosslinked (100/0; 90/10 and 80/20) and crosslinked (C100/0; C90/10 and C80/20) PVA/CA electrospun mats; and b) PVA, CNC powders and uncrosslinked (100/0; 90/10 and 80/20) and crosslinked (C100/0; C90/10 and C80/20) PVA/CNC electrospun mats.

### 3.3 Thermal characterization of the mats

#### 3.3.1 Thermogravimetric analyses

TGA analyses were used to assess three main aspects: (1) the thermal influence of CA and CNC on the polymeric blend; (2) the stability of the electrospun nanofibrous mats after crosslinking; and (3) the effect of the electrospinning and solvent system on the polymers thermal behavior (versus powder-form, unprocessed samples).

TGA and DTG spectra of uncrosslinked and crosslinked PVA-based electrospun nanofibers are depicted in Figure 3. All mats displayed a first common step of mass loss, which was detected at temperatures up to 100 °C (Figures 3a and b), being usually associated with the evaporation of absorbed water molecules, solvents, or the removal of trace amounts of impurities [112]. This first step denounces the hydrophobic and hydrophilic nature of the polymers and could also indicate the formation of bonds between the hydroxyl groups of PVA, CA and CNC with the aldehyde groups of GA. Considering that CA is more hydrophobic than CNC, because of the acetyl groups content, the first mass loss reported on CA-loaded nanofibers occurred at  $\approx 55$  °C, while CNC-containing mats reported it later at  $\approx 90$  °C. In addition, this first mass loss registered for the crosslinked electrospun mats was at lower temperatures compared to the uncrosslinked, indicating the lower availability of free -OH groups.

The second degradation plot, detected between the first mass loss temperature and up to 180 °C, easily seen on the DTG curves of Figure 3 and Figure S3 in the Supporting Information file, referred to the unreacted GA as its boiling point at 25% in water-based solutions is around 101 °C [113,114]. As expected, this step was only found on crosslinked mats. After this point, the main degradation events associated with each polymer were identified. According to the literature, two major steps of weight loss are described for PVA (main component of the electrospun mats), being dependent on the chemical characteristics of the polymer, such as hydrolysis level and molecular weight [115,116]. Here, all electrospun mats revealed two main degradation steps. The first started at around 200 °C extending up to 385 °C, while the second main step occurred between 385 and 510 °C. These have been frequently associated with the polymer side chain (which releases acetyl groups) and main chain decomposition, respectively [45,117]. With the introduction of the cellulose derivatives, CA and CNC, an improvement on the mats' thermal stability was observed (Figure 3 a<sub>1</sub> and b<sub>1</sub>): maximum degradation temperatures were increased, while mass loss was reduced. This phenomenon has been attributed to the strong percolation effect held by the intermolecular hydrogen bonds generated between CA/CNC and PVA [118–122].

Among all mats (without crosslinking), the 80/20 PVA/CA mat revealed the highest degradation temperature, given that CA requires higher temperatures to decompose ( $\approx 364$  °C) than CNC (Figure S3 in Supporting Information file), contributing to a greater thermal stability. Yet, by analyzing the 80/20 PVA/CNC thermal profile two peaks were seen, one around 311 °C and another around 356 °C (Figure 3 b<sub>1</sub>). The first one relates to the amount of the 20% CNC that degrades at  $\approx 303$  °C (Figure S3), whereas the second peak of this main degradation step revealed the percolation effect registered between PVA and CNC, which increased the main degradation temperature compared to 100/0 and 90/10 PVA/CNC. For these CNC-loaded electrospun mats, the beginning of the main degradation step was verified at lower temperature ( $\approx 150$  °C) than that for CA-loaded electrospun mats ( $\approx 180$  °C). This earlier mass loss identified for CNC-containing mats has been attributed to the catalytic effect of the sulfate groups of CNC [27,115,123].

In both formulations (PVA/CA and PVA/CNC), crosslinking improved the thermal stability of the mats (Figure 3). Electrospun mats subjected to crosslinking registered a smaller mass loss during the main degradation steps and a higher maximum degradation temperature compared to equal formulations without crosslinking. These behavior alterations attest to the crosslinking efficiency in establishing interactions between aldehyde and hydroxyl groups and forming a polymer network of enhanced stability. It is noteworthy that only crosslinked neat PVA electrospun mats evidenced an earlier main degradation step (at  $\approx 30$  °C) compared to those uncrosslinked. This may demonstrate that

the neat PVA mats suffered a slight structural change due to the heat provided during crosslinking (60 °C by 7 h), since the acetal bonds formed could have generated spaces along the structure affecting its vulnerability to high temperatures. This result highlighted the importance of cellulose derivatives on the structural stability of the electrospun mats, by guaranteeing strong percolation effects between intermolecular hydrogen bonds.

TGA and DTG spectra evidencing the differences of thermal behavior between electrospun mats and the powder form of polymers were also collected (Figure S3 of Supporting Information file). The first difference is related to moisture evaporation; it was higher on the electrospun nanofibers than on the powder due to the porous structure of the mats, large surface area for molecule binding, and possible presence of remaining solvent molecules. Another change observed is the reduction of maximum mass loss from 340 °C for powder PVA to 309 °C and 317 °C for 100/0 PVA/CA and PVA/CNC mats, respectively. This decrease was also noted in other studies, being related with the increase of surface area [124,125]. Here, it was also depicted the influence of the applied solvents; a more complete degradation profile (with less residue) was detected for the acetic acid prepared PVA mat. This could be a consequence of the superior organization of the PVA chains in dH<sub>2</sub>O due to stronger inter- and intramolecular interactions generated between the -OH groups from dH<sub>2</sub>O and those present in the PVA chains (hydrogen bonding) [126,127].

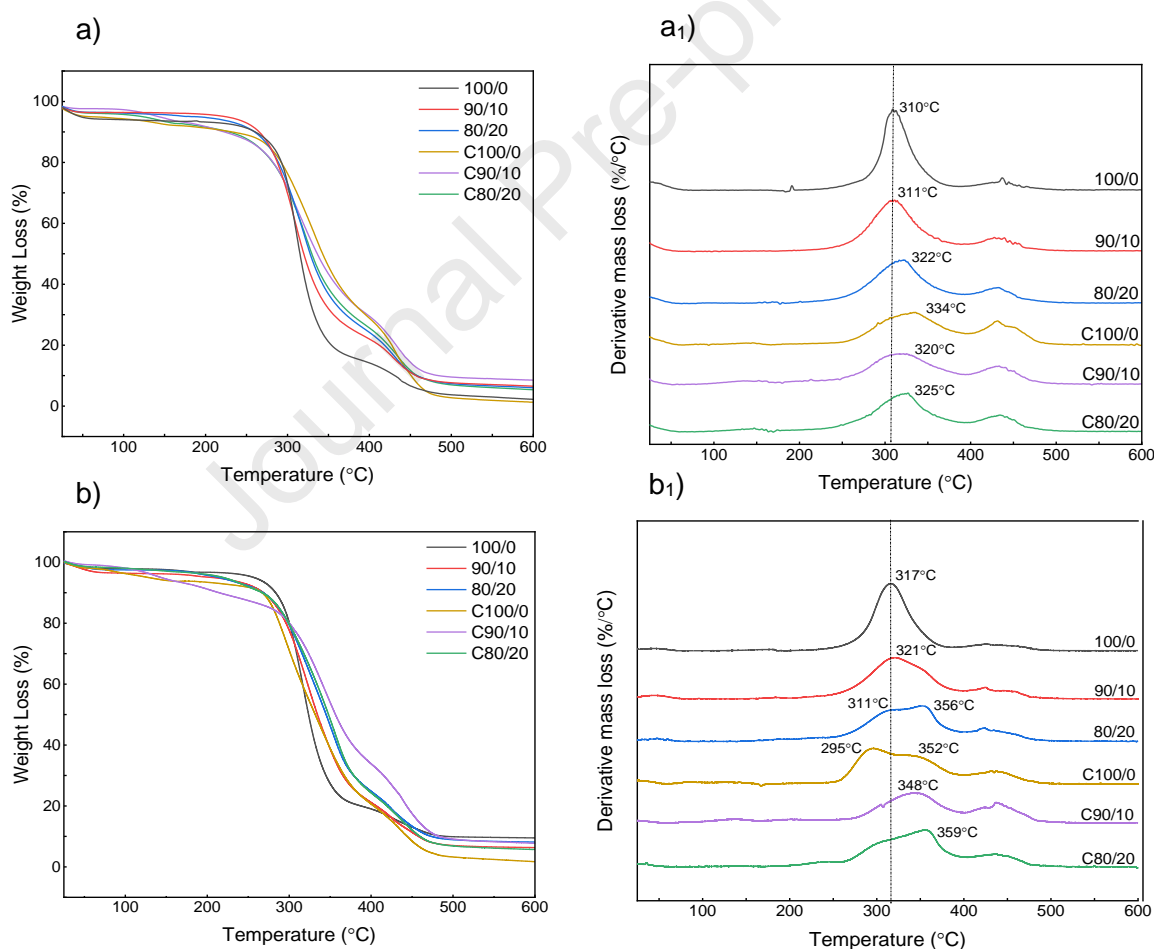


**Figure 3:** TGA curves and corresponding derivatives of 100/0, 90/10, 80/20 and C100/0, C90/10, and C80/20 PVA/CA mats (a and a<sub>1</sub>, respectively) and 100/0, 90/10, 80/20 and C100/0, C90/10, and C80/20 PVA/CNC mats (b and b<sub>1</sub>, respectively).

**3.3.2 Differential scanning calorimetry analysis.** DSC evaluations were performed to assess the thermal and structural properties of the CA- and CNC-doped uncrosslinked and crosslinked electrospun mats, with data concerning the glass temperature ( $T_g$ ), melting temperature ( $T_m$ ) and heat of fusion ( $\Delta H_m$ ), being collected from the second heating step after moisture removal (Table 2). Evidence of the excellent miscibility between polymers was obtained by detecting a single  $T_g$  and a single  $T_m$  on all engineered mats [128]. The  $T_g$  detected for 100/0 PVA/CA and 100/0 PVA/CNC electrospun mats, being respectively 74.10 and 70.73 °C, was within acceptable ranges for the PVA employed. Indeed, as it presents a low-to-medium  $M_w$  and a low degree of hydrolysis, the  $T_g$  tends to be lower than for PVA, with higher hydrolyzation, due to the high number of acetyl groups increasing chain mobility [61,129]. The incorporation of cellulose derivatives on the uncrosslinked mats increased the  $T_g$  from 74.10 °C (100 PVA/CA) to 80.83 °C (80/20 PVA/CA) and from 70.73 °C (100 PVA/CNC) to 79.38 °C (80/20 PVA/CNC). This may be attributed to a reduction of PVA chains mobility induced by the formation of strong interactions between this polymer and the cellulose derivatives [130]. On its turn, the  $T_g$  registered for crosslinked mats was lower comparatively to those uncrosslinked, as shown in Table 2. This is expected since a disorganized, network of acetal bonds is formed between polymers and GA, leading to an increment in the space between polymer chains, hence promoting a plasticization effect [88,131]. A wide  $T_m$  peak was noted for powders and all electrospun mats. By being a wide and unsharp peak, it was demonstrated that all tested materials did not possess a wide ordered crystalline structure, as confirmed by XRD analyses [61]. It is also consistent with the type of PVA used. CNC-doped electrospun mats exhibited higher  $T_m$  and  $\Delta H_m$  than CA-containing mats, which could indicate superior bonding strength and smaller impact on structural organization, as evidenced by XRD results, particularly on the 80/20 formulations [26,132,133].

Crosslinked mats registered a slightly lower  $T_m$  (except for 100/0 and 90/10 PVA/CA mats) and  $\Delta H_m$  than uncrosslinked. This reduction demonstrates that interactions with GA affect the crystallites size and thickness, perturbs structural organization, and, thus, the polymers' degree of crystallinity. As GA is an aldehyde, it can lead PVA to branch, increasing the space between polymer chains. XRD analyses corroborate these DSC conclusions. Furthermore, these data attested, once again, to the efficiency of the crosslinking process employed.

**Table 2:** Main DSC transitions, temperature of main degradations and crystallinity degree  $X_c$  (%) to PVA, CA and CNC powders and for both formulations of electrospun mats.

	Sample code	$T_g$ (°C)	$T_m$ (°C)	$\Delta H$ (J g <sup>-1</sup> )	T peaks of first derivative (°C) (1 <sup>st</sup> peak)	T peaks of first derivative (°C) (2 <sup>nd</sup> peak)	$X_c$ (%)
PVA Powder	-	74.28	190.14	39.18	340	426	30.5
CA Powder	-	-	193.37	14.31	363	-	20.6
CNC Powder	-	-	144.92	171.60	304	-	48.9
PVA 100/0	100/0	74.10	187.1	44.79	310	430	28.8



	<b>90/10</b>	69.70	153.9	10.27	311	430	30.7
	<b>80/20</b>	80.83	185.9	29.90	322	430	18.1
	<b>C100/0</b>	61.01	188.8	6.230	334	430	26.1
	<b>C90/10</b>	68.75	155.3	28.58	320	434	26.2
	<b>C80/20</b>	68.41	159.5	22.73	325	434	16.7
<b>PVA/CNC</b>	<b>100/0</b>	70.73	190.00	50.02	317	426	23.9
	<b>90/10</b>	72.08	191.86	38.91	321	426	25.1
	<b>80/20</b>	79.38	191.81	39.77	311/356	424	30.8
	<b>C100/0</b>	64.65	173.00	43.35	295/352	438	23.0
	<b>C90/10</b>	53.55	170.29	26.32	348	438	23.7
	<b>C80/20</b>	64.33	159.93	22.23	302/359	445	18.7

### 3.4 Evaluation of mechanical properties

#### 3.4.1 Uniaxial tensile tests

Nanofibrous mats engineered for wound dressing applications should display mechanical resistance and flexibility to better respond to clinical demands and patient handling, to efficiently assist the healing process [134]. Young's modulus, UTS and strain at failure of neat PVA mats and CA/CNC-reinforced mats were measured in tensile mode (Table 3). The mechanical performance of electrospun mats is directly influenced by the polymers' chains and polymer-polymer bonding, level of crystallinity, fibers' diameter and morphology, the slip of one fiber over the other during assembly in the collector, and orientation of the nanofibers on the mat [135,136]. Generally, electrospun fibers have demonstrated a higher Young's modulus than other fiber constructs due to their greater structural orientation and crystallinity, obtained in response to the intensive electrical field that acts on the polymer jet during extrusion, turning it more elongated and organized [137,138].

Usually, PVA mats behave as soft materials, with relatively high strain and low stiffness [106,124]. Data from Table 3 corroborates this statement (namely the neat PVA mats). Studies have related this superior elongation at break to the viscosities of polymeric solutions, which increase proportionally to the amount of intra- and intermolecular bonds generated between polymer chains [126,139]. Here, both neat PVA solutions, prepared with two distinct solvent systems, showed the highest viscosities from the tested group (Table 1), which may explain the enhanced capacity of deformation of these mats comparatively to those reinforced with cellulose derivatives. The effect of the solvent system was also evident on the Young's moduli and UTS properties, which were raised by the use of acetic acid comparatively to 100% dH<sub>2</sub>O (lower solution viscosity).

The addition of CA and CNC to the blend, enhanced the mats' Young's modulus, therefore acquiring greater elastic capacity, even superior to some commercial dressings referenced in literature [140,141]. The CNC impact was more important than that of CA. CNC has been considered one of the strongest and stiffest polymers in nature [142]. It is frequently used to reinforce the mechanical properties of polymer materials due to its high elastic modulus and mechanical strength resultant from its densely and orderly crystallized structural organization obtained after acid hydrolysis [45,143]. Additionally, CNC allows the efficient stress transfer from soft PVA matrix to stiff CNC additives due to the surface charges present [144,145]. Such reinforcement also benefits from the strong mechanical percolation between the PVA matrix and the CNC, through hydrogen bonding, promoting the formation of a rigid interconnected network that resists the tensile stress employed [145,146]. Moreover, during electrospinning, and because of the electric field applied, CNC can be dispersed evenly throughout the PVA matrix, raising the polymers' interfacial adhesion [147].

On the other hand, CA influenced the most the mats' UTS and strain at failure, as easily seen in Figure S4 of the Supporting Information file [114]. With the addition of 10% CA and even CNC, an increase in UTS was observed, meaning that the mats became more likely to prevent crack propagation when reinforced with the cellulose derivatives [148]. However, as the percentage of these compounds in the blend increased to 20%, the tensile strength and strain at failure decreased, particularly in the

PVA/CNC formulation. Other researchers have reported similar outcomes [45,123,138,140,149]. This can be explained by the appearance of interruptions along the PVA chains as a result of the introduction of such additives. Data suggests that for the incorporation of CA and CNC to be effective, and establish strong bonds with PVA, it must be between specific limits that, once surpassed, lead to the polymer structure disorganization and destabilization [45].

After crosslinking, neat PVA mats reported once again the influence of the solvent system employed in the solutions preparation (Table 3). In the presence of acetic acid, C100/0 PVA/CA mats lost elastic capacity from 0.485 to 0.363, while the C100/0 PVA/CNC prepared only with dH<sub>2</sub>O increased from 0.297 to 1.057 MPa. Acetic acid may compromise these properties on crosslinked samples since optimal reactivity conditions have been linked to neutral or basic environments [150]. Regarding the Young's modulus, both CA and CNC-containing crosslinked electrospun mats registered a slight decrease after processing with GA. The only exception to this tendency was noted for the C80/20 PVA/CA electrospun mats, in which the opposite occurred ( $p > 0.05$ , non-significant). Most crosslinked mats also reported a reduction in UTS (C80/20 PVA/CA was the only exception;  $p > 0.05$ , non-significant). These results mean that the established acetal bonds formed after crosslinking reduced the materials maximum capacity to withstand stretching before breaking. These also denote well the great efficiency of the crosslinking process between the polymers and GA. Regarding the strain at failure, from all tested combinations, the C100/0 mats (both PVA/CA and PVA/CNC) were the ones that experience the greatest decline (Table 3). Once again, the strength of the acetal bonds generated after crosslinking is evidenced, leading the mats to become more resistant to deformation. Lower tensile strain after GA crosslinking is also attributable to reduced molecular mobility within the polymer network [151]. Among the crosslinked mats, the C90/10 and C80/20 PVA/CA were the ones with the highest deformation capacity. Even though CA has been identified as far from excellent when it comes to mechanical resilience [152], the combination with PVA appear to have altered that character. Therefore, the acetal bonds formed between PVA/CA and GA, even though not as frequent as within C100/0 mats due to the higher amount of hydroxyl groups, may have improved the strain capacity of the PVA/CA combinations. In general, it was seen that the smaller the number of acetal bonds between PVA and CA the greater the Young's modulus and UTS. This, however, was not an indicative of the CA-containing mats instability in water compared to CNC-loaded mats. In fact, crosslinked PVA/CA mats maintained their structural integrity in aqueous environment both via these acetal bonds and the hydrophobicity of the CA acetate groups (39.8 wt.% acetyl content) [2,153,154].

An ideal wound dressing material, together with the appropriate mechanical resistance and elasticity to prevent potential additional harm on the injured site, must match the biomechanical characteristics of the underlying skin tissue [128]. According to the literature, the Young's modulus of human skin ranges from 0.1 to 10 MPa, the UTS from 0.1 to 32 MPa, and strain at failure ranges from 17 to 207% [55,128,129]. In this way, most results obtained are within the acceptable ranges for the application, even after crosslinking; the only exception being the 80/20 PVA/CNC electrospun mats that presented very low strain at failure (both before and after crosslinking).

**Table 3:** Young's modulus, UTS and strain at failure of PVA/CA and PVA/CNC electrospun mats, evaluated at a displacement rate of 3.0 mm/min. Data are expressed as mean  $\pm$  SD. Statistical significance between mats was inexistant (Kruskal-Wallis test).

	Sample code	Young's Modulus (MPa)	UTS (MPa)	Strain at Failure (%)
PVA/CA	<b>100/0</b>	0.485 $\pm$ 0.031	9.624 $\pm$ 2.463	43.881 $\pm$ 1.354
	<b>90/10</b>	0.851 $\pm$ 0.518	14.839 $\pm$ 9.428	31.480 $\pm$ 5.934
	<b>80/20</b>	0.722 $\pm$ 0.197	4.032 $\pm$ 1.950	26.758 $\pm$ 5.057
	<b>C100/0</b>	0.363 $\pm$ 0.156	4.799 $\pm$ 1.766	20.502 $\pm$ 5.272
	<b>C90/10</b>	0.415 $\pm$ 0.190	3.647 $\pm$ 2.438	34.329 $\pm$ 15.039

PVA/CNC	<b>C80/20</b>	1.362 ± 0.295	13.651 ± 2.547	36.114 ± 0.732
	<b>100/0</b>	0.297 ± 0.051	3.913 ± 0.783	48.801 ± 10.708
	<b>90/10</b>	1.180 ± 0.457	6.109 ± 3.618	29.188 ± 10.654
	<b>80/20</b>	2.051 ± 0.929	2.538 ± 1.386	2.188 ± 1.165
	<b>C100/0</b>	1.057 ± 0.331	3.534 ± 0.926	20.314 ± 7.416
	<b>C90/10</b>	1.162 ± 0.152	4.532 ± 0.586	18.045 ± 7.729
	<b>C80/20</b>	1.601 ± 0.111	1.466 ± 0.515	4.480 ± 0.208

### 3.4.2 Dynamic mechanical analysis

The thermomechanical properties of the electrospun nanofibrous mats were analyzed by DMA, performed in tensile mode under temperatures up to 200 °C and a fixed frequency of 1 Hz. Figure 4 shows the storage modulus ( $E'$ , elastic response) versus temperature, while Table 4 presents the  $E'$  values at 37 °C as this intends to mimic the temperature of the physiological conditions. At low temperatures (< 37 °C), the  $E'$  reported constant values for most tested materials in the glassy region due to low chain mobility (Figure 4) [56,103]. At 37 °C, the solvents influence became again evident: neat PVA/CA electrospun mats prepared with acetic acid/dH<sub>2</sub>O reported  $E'$  of 214.22 MPa, which settled in 185.54 MPa after crosslinking. On its turn, 100/0 PVA/CNC mats prepared solely with water only reached 14.56 MPa, dropping to 11.34 MPa after crosslinking. These values showed that the neat PVA mats prepared with acetic acid had the ability to store more elastic energy, meaning that there was formation of more efficient and organized intermolecular bonds between the polymers in this formulation [155]. These data are corroborated with the  $X_c$  (%) values obtained from XRD analyses (table 2), as the 100/0 mats produced with acetic acid displayed superior crystallinity than those produced with just distilled water ( $E'$  is directly influenced by crystallinity). Unlike neat PVA, most cellulose derivatives-containing mats experienced an increment in their elastic capacity after crosslinking (rise of  $E'$  at 37°C). Data indicates that the acetal bonds formed in these formulations may not have harmed the structure of the mat as much as those at C100/0, and that the molecular motions were largely restricted to vibration and short-range rotation either due to these convenient acetal bonds or to the presence of the cellulose derivatives along the PVA chains [156].

At increasing temperatures (> 37 °C), uncrosslinked 100/0 electrospun mats revealed two salient peaks (Figure 4). The first peak is the most important as it is linked to a sub-T<sub>g</sub> (secondary relaxation), which occurs in response to the reorganization of the hydrogen bonding in the amorphous region of the polymer or due to conformational changes within the PVA side groups [60,129]. In the 100/0 PVA/CA this peak was detected at ≈ 40.34 °C and for PVA/CNC electrospun mats it was seen at ≈ 44.95 °C, both in accordance with a study done by Cassu et al. [129]. In the CA and CNC-containing electrospun mats, this first peak appeared slightly camouflaged, but at higher temperatures (Table 4) since the additives hindered polymer chain movement [56,60]. It evidenced the greater difficulty experienced by the PVA side groups in undergoing conformational changes in the presence of cellulose derivatives. On its turn, crosslinked mats registered a lower temperature for this sub-T<sub>g</sub> transition. It could be related with the structural disorganization GA confers to the mats, as referred in the DSC evaluations. At around 64 °C, the uncrosslinked 100/0 PVA electrospun mats reported a transition with a sharp drop in  $E'$ ; this is frequently associated to the glass-rubber T<sub>g</sub> of 88% hydrolyzed PVA [60]. The same tendency of increasing sub-T<sub>g</sub> temperatures with higher amounts of cellulose derivatives was evidenced also on the T<sub>g</sub> evaluations. This increase has been related to the hydrogen bonds established between PVA and CA/CNC, highlighting their strength and consequent reduced flexibility and mobility of the PVA polymeric chains [106,157,158]. An improvement on the mats'  $E'$  modulus with increasing CA and CNC contents was also registered (Table 4), being this increment related with limited movement of the PVA chains and with the efficient stress transfer from soft PVA matrix to CA and to the stiff CNC. Uncrosslinked 80/20 PVA/CNC mats reached the highest  $E'$  from the group, at 742.04 MPa, due to the recognized superior crystallinity of CNC (confirmed by XRD results), being these data also in line with the Young's modulus assessments. After crosslinking, the mats'  $E'$  values

decreased. These observations are also supported by XRD and DSC data, which evidenced a reduction in the mats' crystallinity [159]. Like the sub-Tg, the Tg's determined for most crosslinked mats were inferior to the uncrosslinked. This reflects a higher structural disorganization and, consequently, a lower E' modulus [88].

At temperatures between Tg and 200 °C, a constant drop in the E' modulus was observed. It can be ascribed to motions of the polymer chains, which lead to irreversible polymeric chain flow and disentanglement that are typical in amorphous polymers [103].

**Table 4:** Secondary relaxation temperature (Ts), glass transition temperature (Tg) and storage modulus (E') at 37° C and at maximum peaks for PVA/CA and PVA/CNC electrospun mats.

	Sample code	E' (MPa) (37°C)	Sub-Tg (°C)	E' (MPa)	Tg (°C)	E' (MPa)
PVA/CA	100/0	214.22	40.34	241.08	62.37	147.02
	90/10	24.37	69.26	31.61	99.76	43.32
	80/20	65.48	55.49	264.87	76.25	235.70
	C100/0	185.54	37.62	251.59	43.40	188.65
	C90/10	77.17	62.47	86.90	79.91	163.74
	C80/20	48.44	58.62	116.78	73.20	195.29
PVA/CNC	100/0	14.56	44.95	85.23	64.06	81.22
	90/10	26.27	50.16	154.16	64.79	238.99
	80/20	130.41	-	-	82.60	742.04
	C100/0	11.34	40.58	10.95	74.80	14.52
	C90/10	29.54	47.30	38.95	64.79	70.25
	C80/20	188.09	50.06	446.17	66.74	433.33

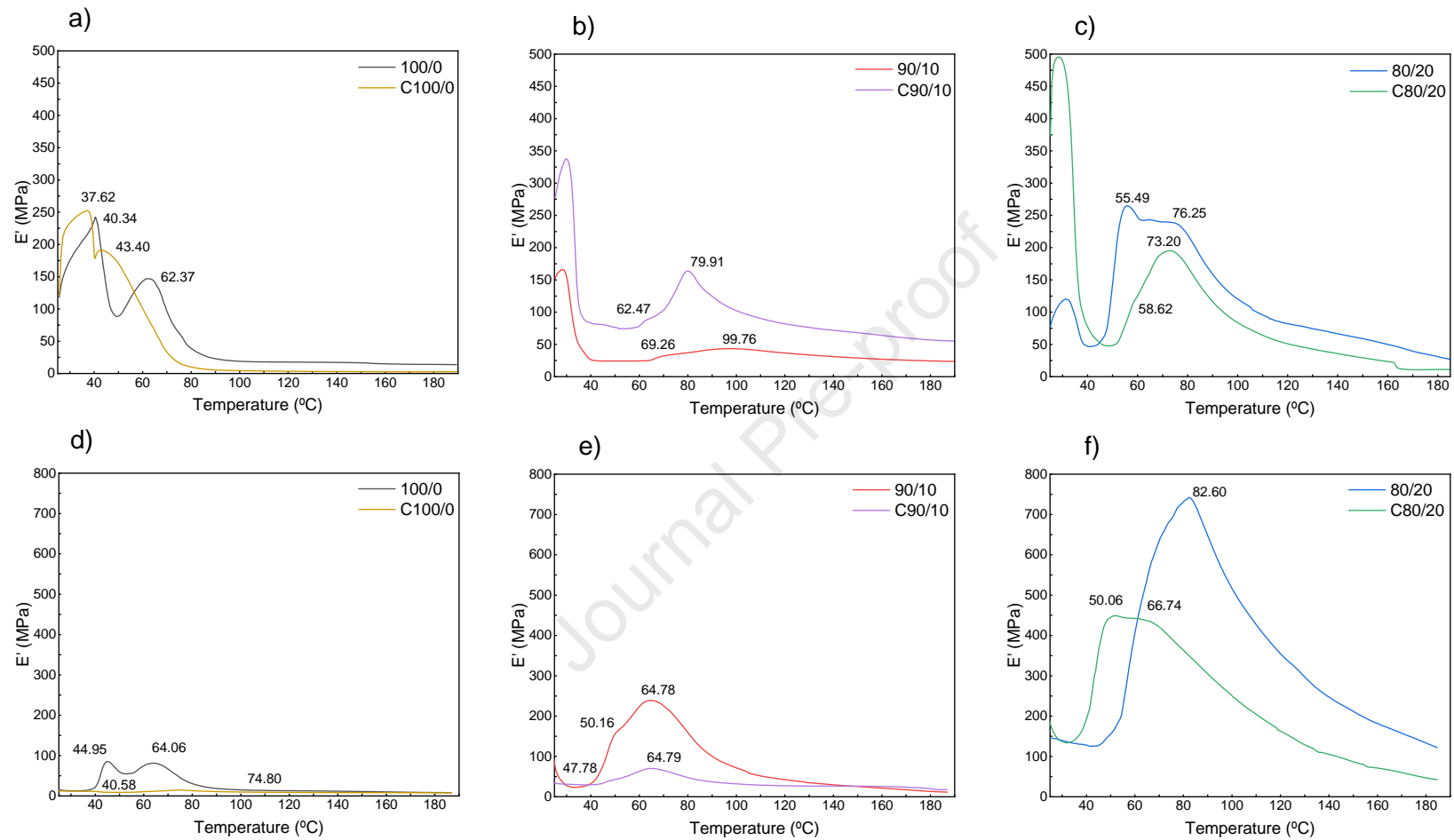


**Figure 4:** The curves of storage modulus ( $E'$ ) versus temperature of (a, b and c) PVA/CA and (d, e and f) PVA/CNC uncrosslinked and crosslinked electrospun mats.

#### 4. Conclusions

Flexible, uniform, porous PVA/CA, and PVA/CNC electrospun mats were successfully produced via electrospinning for prospective uses as dressings in CW care. Thermal analysis demonstrated that the incorporation of cellulose derivatives, CA, and CNC, improved the mats' thermal stability by increasing the maximum degradation temperatures, while the mass loss was reduced. Data also confirmed the excellent miscibility and strong bonding between polymers, as evidenced by the increasing T<sub>g</sub> and T<sub>m</sub>. These characteristics were also noticeable on the mechanical assessments, which also verified the stiffness of the CNC. The Young's modulus increased with the addition of these cellulose derivatives, while the elongation capacity decreased because of the interruption of the soft and high strained PVA chains. After crosslinking, the thermal stability of the mats was improved. Crosslinked electrospun mats registered smaller mass losses during the main degradation steps and higher maximum degradation temperatures than equal formulations without crosslinking. However, a more disorganized structure was noted by lower melting temperatures, enthalpy values and crystallinity, and as consequence Young's modulus, UTS, strain at failure and E' modulus decreased. All examinations demonstrated the importance of cellulose derivatives on the structural stability of the electrospun mats. Importantly, most of the developed electrospun mats (except for C80/20 PVA/CNC mat due to low strain at failure) were deemed appropriate for applications as wound dressings.

#### Acknowledgments

Authors acknowledge the Portuguese Foundation for Science and Technology (FCT), FEDER funds by means of Portugal 2020 Competitive Factors Operational Program (POCI) and the Portuguese Government (OE) for funding the project with reference PTDC/CTM-TEX/28074/2017 (POCI-01-0145-FEDER-028074). Authors also acknowledge project UIDP/00264/2020 of Centre for Textile Science and Technology (2C2T), funded by national funds through FCT/MCTES. M.A.T., D.P.F and H.P.F. also acknowledge FCT for PhD scholarship (SFRH/BD/148930/2019) and junior (CEECIND/02803/2017) and auxiliary researcher (2021.02720.CEECIND) contracts, respectively.

#### 5. Bibliography

- [1] A.S. Ribeiro, S.M. Costa, D.P. Ferreira, R.C. Calhelha, L. Barros, D. Stojković, M. Soković, I.C.F.R. Ferreira, R. Fangueiro, Chitosan/nanocellulose electrospun fibers with enhanced antibacterial and antifungal activity for wound dressing applications, *React Funct Polym.* 159 (2021) 104808. <https://doi.org/10.1016/j.reactfunctpolym.2020.104808>.
- [2] M.A. Teixeira, M.C. Paiva, M.T.P. Amorim, H.P. Felgueiras, Electrospun Nanocomposites Containing Cellulose and Its Derivatives Modified with Specialized Biomolecules for an Enhanced Wound Healing, *Nanomaterials.* 10 (2020) 557. <https://doi.org/10.3390/nano10030557>.
- [3] Y. Hussein, E.M. El-Fakharany, E.A. Kamoun, S.A. Loutfy, R. Amin, T.H. Taha, S.A. Salim, M. Amer, Electrospun PVA/hyaluronic acid/L-arginine nanofibers for wound healing applications: Nanofibers optimization and in vitro bioevaluation, *Int J Biol Macromol.* 164 (2020) 667–676. <https://doi.org/10.1016/j.ijbiomac.2020.07.126>.
- [4] E. Naseri, A. Ahmadi, A review on wound dressings: Antimicrobial agents, biomaterials, fabrication techniques, and stimuli-responsive drug release, *Eur Polym J.* 173 (2022) 111293. <https://doi.org/10.1016/j.eurpolymj.2022.111293>.

- [5] E. Rezvani Ghomi, F. Khosravi, R.E. Neisiany, M. Shakiba, M. Zare, R. Lakshminarayanan, V. Chellappan, M. Abdouss, S. Ramakrishna, Advances in electrospinning of aligned nanofiber scaffolds used for wound dressings, *Curr Opin Biomed Eng.* 22 (2022) 100393. <https://doi.org/10.1016/j.cobme.2022.100393>.
- [6] M.A. Teixeira, M.T.P. Amorim, H.P. Felgueiras, Poly(Vinyl Alcohol)-Based Nanofibrous Electrospun Scaffolds for Tissue Engineering Applications, *Polymers (Basel)*. 12 (2019) 7. <https://doi.org/10.3390/polym12010007>.
- [7] M.A. Teixeira, J.C. Antunes, M.T.P. Amorim, H.P. Felgueiras, Green Optimization of Glutaraldehyde Vapor-Based Crosslinking on Poly(Vinyl Alcohol)/Cellulose Acetate Electrospun Mats for Applications as Chronic Wound Dressings, in: *The First International Conference on “Green” Polymer Materials 2020*, MDPI, Basel Switzerland, 2020: p. 30. <https://doi.org/10.3390/CGPM2020-07193>.
- [8] H.P. Felgueiras, M.A. Teixeira, T.D. Tavares, N.C. Homem, A. Zille, M.T.P. Amorim, Antimicrobial action and clotting time of thin, hydrated poly(vinyl alcohol)/cellulose acetate films functionalized with LL37 for prospective wound-healing applications, *J Appl Polym Sci.* 137 (2020) 48626. <https://doi.org/10.1002/app.48626>.
- [9] H.P. Felgueiras, M.A. Teixeira, T.D. Tavares, M.T.P. Amorim, New method to produce poly(vinyl alcohol)/cellulose acetate films with improved antibacterial action, *Mater Today Proc.* (2020) 10–13. <https://doi.org/10.1016/j.matpr.2019.12.100>.
- [10] S. Sun, M. Hao, C. Ding, J. Zhang, Q. Ding, Y. Zhang, Y. Zhao, W. Liu, SF/PVP nanofiber wound dressings loaded with phlorizin: preparation, characterization, in vivo and in vitro evaluation, *Colloids Surf B Biointerfaces.* 217 (2022) 112692. <https://doi.org/10.1016/j.colsurfb.2022.112692>.
- [11] E. Naseri, A. Ahmadi, A review on wound dressings: Antimicrobial agents, biomaterials, fabrication techniques, and stimuli-responsive drug release, *Eur Polym J.* 173 (2022) 111293. <https://doi.org/10.1016/j.eurpolymj.2022.111293>.
- [12] M.K. Selatile, S.S. Ray, V. Ojijo, R. Sadiku, Recent developments in polymeric electrospun nanofibrous membranes for seawater desalination, *RSC Adv.* 8 (2018) 37915–37938. <https://doi.org/10.1039/C8RA07489E>.
- [13] B. Yan, Y. Zhang, Z. Li, P. Zhou, Y. Mao, Electrospun nanofibrous membrane for biomedical application, *SN Appl Sci.* 4 (2022) 172. <https://doi.org/10.1007/s42452-022-05056-2>.
- [14] M. Liu, X.-P. Duan, Y.-M. Li, D.-P. Yang, Y.-Z. Long, Electrospun nanofibers for wound healing, *Materials Science and Engineering: C.* 76 (2017) 1413–1423. <https://doi.org/10.1016/j.msec.2017.03.034>.
- [15] I. Behere, G. Ingavle, *In vitro* and *in vivo* advancement of multifunctional electrospun nanofiber scaffolds in wound healing applications: Innovative nanofiber designs, stem cell approaches, and future perspectives, *J Biomed Mater Res A.* 110 (2022) 443–461. <https://doi.org/10.1002/jbm.a.37290>.

- [16] Y. Yang, Y. Du, J. Zhang, H. Zhang, B. Guo, Structural and Functional Design of Electrospun Nanofibers for Hemostasis and Wound Healing, *Advanced Fiber Materials*. (2022). <https://doi.org/10.1007/s42765-022-00178-z>.
- [17] E. Rezvani Ghomi, S. Khalili, S. Nouri Khorasani, R. Esmaeely Neisiany, S. Ramakrishna, Wound dressings: Current advances and future directions, *J Appl Polym Sci*. 136 (2019) 47738. <https://doi.org/10.1002/app.47738>.
- [18] W. Chen, Z. Gao, M. He, Y. Dou, G. Yin, J. Ding, Vapor-phase glutaraldehyde crosslinked waste protein-based nanofiber nonwovens as an environmentally friendly wound dressing, *React Funct Polym*. 172 (2022) 105203. <https://doi.org/10.1016/j.reactfunctpolym.2022.105203>.
- [19] N. Bahari, N. Hashim, A. Md Akim, B. Maringgal, Recent Advances in Honey-Based Nanoparticles for Wound Dressing: A Review, *Nanomaterials*. 12 (2022) 2560. <https://doi.org/10.3390/nano12152560>.
- [20] X. Wang, B. Ding, B. Li, Biomimetic electrospun nanofibrous structures for tissue engineering, *Materials Today*. 16 (2013) 229–241. <https://doi.org/10.1016/j.mattod.2013.06.005>.
- [21] E.R. Ghomi, S. Khalili, S.N. Khorasani, R.E. Neisiany, Wound dressings : Current advances and future directions, *Applied Polymer*. 47738 (2019) 1–12. <https://doi.org/10.1002/app.47738>.
- [22] M. Calzado-Delgado, M.O. Guerrero-Pérez, K.L. Yeung, A new versatile x–y–z electrospinning equipment for nanofiber synthesis in both far and near field, *Sci Rep*. 12 (2022) 4872. <https://doi.org/10.1038/s41598-022-08310-0>.
- [23] S.M. Tan, X.Y. Teoh, J. le Hwang, Z.P. Khong, R. Sejare, A.Q. Almashhadani, R.A. Assi, S.Y. Chan, Electrospinning and its potential in fabricating pharmaceutical dosage form, *J Drug Deliv Sci Technol*. 76 (2022) 103761. <https://doi.org/10.1016/j.jddst.2022.103761>.
- [24] S. Liu, S. Qin, M. He, D. Zhou, Q. Qin, H. Wang, Current applications of poly(lactic acid) composites in tissue engineering and drug delivery, *Compos B Eng*. 199 (2020) 108238. <https://doi.org/10.1016/j.compositesb.2020.108238>.
- [25] K. Peranidze, T. v. Safronova, N.R. Kildeeva, Fibrous Polymer-Based Composites Obtained by Electrospinning for Bone Tissue Engineering, *Polymers (Basel)*. 14 (2021) 96. <https://doi.org/10.3390/polym14010096>.
- [26] M.A. Teixeira, J.C. Antunes, C.L. Seabra, S.D. Tohidi, S. Reis, M.T.P. Amorim, H.P. Felgueiras, Tiger 17 and pexiganan as antimicrobial and hemostatic boosters of cellulose acetate-containing poly(vinyl alcohol) electrospun mats for potential wound care purposes, *Int J Biol Macromol*. 209 (2022) 1526–1541. <https://doi.org/10.1016/j.ijbiomac.2022.04.130>.
- [27] M.A. Teixeira, J.C. Antunes, C.L. Seabra, A. Fertuzinhos, S.D. Tohidi, S. Reis, M.T.P. Amorim, D.P. Ferreira, H.P. Felgueiras, Antibacterial and hemostatic capacities of cellulose nanocrystalline-reinforced poly(vinyl alcohol) electrospun mats doped with Tiger 17 and pexiganan peptides for prospective wound healing



- applications, *Biomaterials Advances*. 137 (2022) 212830. <https://doi.org/10.1016/j.bioadv.2022.212830>.
- [28] H. Adeli, M.T. Khorasani, M. Parvazinia, Wound dressing based on electrospun PVA/chitosan/starch nanofibrous mats: Fabrication, antibacterial and cytocompatibility evaluation and in vitro healing assay, *Int J Biol Macromol*. 122 (2019) 238–254. <https://doi.org/10.1016/j.ijbiomac.2018.10.115>.
- [29] M. Gazzano, C. Gualandi, A. Zucchelli, T. Sui, A.M. Korsunsky, C. Reinhard, M.L. Focarete, Structure-morphology correlation in electrospun fibers of semicrystalline polymers by simultaneous synchrotron SAXS-WAXD, *Polymer (Guildf)*. 63 (2015) 154–163. <https://doi.org/10.1016/j.polymer.2015.03.002>.
- [30] J. Ayutsede, M. Gandhi, S. Sukigara, H. Ye, C. Hsu, Y. Gogotsi, F. Ko, Carbon Nanotube Reinforced *Bombyx mori* Silk Nanofibers by the Electrospinning Process, *Biomacromolecules*. 7 (2006) 208–214. <https://doi.org/10.1021/bm0505888>.
- [31] J.-P. Jeun, Y.-K. Jeon, Y.-C. Nho, P.-H. Kang, Effects of gamma irradiation on the thermal and mechanical properties of chitosan/PVA nanofibrous mats, *Journal of Industrial and Engineering Chemistry*. 15 (2009) 430–433. <https://doi.org/10.1016/j.jiec.2009.02.001>.
- [32] M. Kancheva, A. Toncheva, N. Manolova, I. Rashkov, Enhancing the mechanical properties of electrospun polyester mats by heat treatment, *Express Polym Lett*. 9 (2015) 49–65. <https://doi.org/10.3144/expresspolymlett.2015.6>.
- [33] S. Nauman, G. Lubineau, H.F. Alharbi, Post Processing Strategies for the Enhancement of Mechanical Properties of ENMs (Electrospun Nanofibrous Membranes): A Review, *Membranes (Basel)*. 11 (2021) 39. <https://doi.org/10.3390/membranes11010039>.
- [34] J. Lee, Y. Deng, Increased mechanical properties of aligned and isotropic electrospun PVA nanofiber webs by cellulose nanowhisker reinforcement, *Macromol Res*. 20 (2012) 76–83. <https://doi.org/10.1007/s13233-012-0008-3>.
- [35] B. Ding, H.-Y. Kim, S.-C. Lee, C.-L. Shao, D.-R. Lee, S.-J. Park, G.-B. Kwag, K.-J. Choi, Preparation and characterization of a nanoscale poly(vinyl alcohol) fiber aggregate produced by an electrospinning method, *J Polym Sci B Polym Phys*. 40 (2002) 1261–1268. <https://doi.org/10.1002/polb.10191>.
- [36] A.Sh. Asran, Khashayar. Razghandi, N. Aggarwal, G.H. Michler, T. Groth, Nanofibers from Blends of Polyvinyl Alcohol and Polyhydroxy Butyrate As Potential Scaffold Material for Tissue Engineering of Skin, *Biomacromolecules*. 11 (2010) 3413–3421. <https://doi.org/10.1021/bm100912v>.
- [37] Y. Yang, H. Hu, Spacer fabric-based exuding wound dressing – Part II: Comparison with commercial wound dressings, *Textile Research Journal*. 87 (2017) 1481–1493. <https://doi.org/10.1177/0040517516654110>.
- [38] N. Naseri, A.P. Mathew, L. Girandon, M. Fröhlich, K. Oksman, Porous electrospun nanocomposite mats based on chitosan–cellulose nanocrystals for

- wound dressing: effect of surface characteristics of nanocrystals, *Cellulose*. 22 (2015) 521–534. <https://doi.org/10.1007/s10570-014-0493-y>.
- [39] Y. Zhong, H. Xiao, F. Seidi, Y. Jin, Natural Polymer-Based Antimicrobial Hydrogels without Synthetic Antibiotics as Wound Dressings, *Biomacromolecules*. 21 (2020) 2983–3006. <https://doi.org/10.1021/acs.biomac.0c00760>.
- [40] Z. Fan, B. Liu, J. Wang, S. Zhang, Q. Lin, P. Gong, L. Ma, S. Yang, A novel wound dressing based on Ag/graphene polymer hydrogel: Effectively kill bacteria and accelerate wound healing, *Adv Funct Mater*. 24 (2014) 3933–3943. <https://doi.org/10.1002/adfm.201304202>.
- [41] B. Vigani, S. Rossi, G. Sandri, M.C. Bonferoni, C.M. Caramella, F. Ferrari, Hyaluronic acid and chitosan-based nanosystems: a new dressing generation for wound care, *Expert Opin Drug Deliv*. 16 (2019) 715–740. <https://doi.org/10.1080/17425247.2019.1634051>.
- [42] Q. Chen, T.K. Sinha, H. Li, W. Li, J.K. Kim, A Facile Approach towards Fabrication of Electrospun Nanofibrous Mats based Multicompartment Wound Dressing Fabric, *Macromol Res*. 26 (2018) 1265–1272. <https://doi.org/10.1007/s13233-019-7028-1>.
- [43] Y. Wang, L. Chen, Cellulose Nanowhiskers and Fiber Alignment Greatly Improve Mechanical Properties of Electrospun Prolamin Protein Fibers, *ACS Appl Mater Interfaces*. 6 (2014) 1709–1718. <https://doi.org/10.1021/am404624z>.
- [44] H.P. Felgueiras, M.A. Teixeira, T.D. Tavares, M.T.P. Amorim, New method to produce poly(vinyl alcohol)/cellulose acetate films with improved antibacterial action, *Mater Today Proc*. 31 (2020) S269–S272. <https://doi.org/10.1016/j.matpr.2019.12.100>.
- [45] S. Huan, L. Bai, W. Cheng, G. Han, Manufacture of electrospun all-aqueous poly(vinyl alcohol)/cellulose nanocrystal composite nanofibrous mats with enhanced properties through controlling fibers arrangement and microstructure, *Polymer (Guildf)*. 92 (2016) 25–35. <https://doi.org/10.1016/j.polymer.2016.03.082>.
- [46] E. Amini, C. Valls, M.B. Roncero, Ionic liquid-assisted bioconversion of lignocellulosic biomass for the development of value-added products, *J Clean Prod*. 326 (2021) 129275. <https://doi.org/10.1016/j.jclepro.2021.129275>.
- [47] E.R.D. Seiler, Y. Takeoka, M. Rikukawa, M. Yoshizawa-Fujita, Development of a novel cellulose solvent based on pyrrolidinium hydroxide and reliable solubility analysis, *RSC Adv*. 10 (2020) 11475–11480. <https://doi.org/10.1039/D0RA01486A>.
- [48] M.A. Teixeira, M.T.P. Amorim, H.P. Felgueiras, Cellulose Acetate in Wound Dressings Formulations: Potentialities and Electrospinning Capability, in: 2020: pp. 1227–1230. [https://doi.org/10.1007/978-3-030-31635-8\\_149](https://doi.org/10.1007/978-3-030-31635-8_149).
- [49] A.G.B. Pereira, A.R. Fajardo, A.P. Gerola, J.H.S. Rodrigues, C. v. Nakamura, E.C. Muniz, Y.-L. Hsieh, First report of electrospun cellulose acetate nanofibers mats

- with chitin and chitosan nanowhiskers: Fabrication, characterization, and antibacterial activity, *Carbohydr Polym.* 250 (2020) 116954. <https://doi.org/10.1016/j.carbpol.2020.116954>.
- [50] M. Oprea, S.I. Voicu, Recent advances in composites based on cellulose derivatives for biomedical applications, *Carbohydr Polym.* 247 (2020) 116683. <https://doi.org/10.1016/j.carbpol.2020.116683>.
- [51] A. Ullah, S. Ullah, M.Q. Khan, M. Hashmi, P.D. Nam, Y. Kato, Y. Tamada, I.S. Kim, Manuka honey incorporated cellulose acetate nanofibrous mats: Fabrication and in vitro evaluation as a potential wound dressing, *Int J Biol Macromol.* 155 (2020) 479–489. <https://doi.org/10.1016/j.ijbiomac.2020.03.237>.
- [52] B. Abubakar Abdulkadir, J. Ojur Dennis, A. Abdullahi Adam, Y. Mudassir Hassan, N. Asyiqin Shamsuri, M.F. Shukur, Preparation and characterization of solid biopolymer electrolytes based on polyvinyl alcohol/cellulose acetate blend doped with potassium carbonate (K<sub>2</sub>CO<sub>3</sub>) salt, *Journal of Electroanalytical Chemistry.* 919 (2022) 116539. <https://doi.org/10.1016/j.jelechem.2022.116539>.
- [53] H. Kargarzadeh, R.M. Sheltami, I. Ahmad, I. Abdullah, A. Dufresne, Cellulose nanocrystal reinforced liquid natural rubber toughened unsaturated polyester: Effects of filler content and surface treatment on its morphological, thermal, mechanical, and viscoelastic properties, *Polymer (Guildf).* 71 (2015) 51–59. <https://doi.org/10.1016/j.polymer.2015.06.045>.
- [54] J. Shojaeiarani, D.S. Bajwa, S. Chanda, Cellulose nanocrystal based composites: A review, *Composites Part C: Open Access.* 5 (2021) 100164. <https://doi.org/10.1016/j.jcomc.2021.100164>.
- [55] S. Huan, L. Bai, W. Cheng, G. Han, Manufacture of electrospun all-aqueous poly(vinyl alcohol)/cellulose nanocrystal composite nanofibrous mats with enhanced properties through controlling fibers arrangement and microstructure, *Polymer (Guildf).* 92 (2016) 25–35. <https://doi.org/10.1016/j.polymer.2016.03.082>.
- [56] H.F. Alharbi, M. Luqman, H. Fouad, K.A. Khalil, N.H. Alharthi, Viscoelastic behavior of core-shell structured nanofibers of PLA and PVA produced by coaxial electrospinning, *Polym Test.* 67 (2018) 136–143. <https://doi.org/10.1016/j.polymertesting.2018.02.026>.
- [57] A. Ullah, S. Ullah, M.Q. Khan, M. Hashmi, P.D. Nam, Y. Kato, Y. Tamada, I.S. Kim, Manuka honey incorporated cellulose acetate nanofibrous mats: Fabrication and in vitro evaluation as a potential wound dressing, *Int J Biol Macromol.* 155 (2020) 479–489. <https://doi.org/10.1016/j.ijbiomac.2020.03.237>.
- [58] A.C.M. Cidreira, K.C. de Castro, T. Hatami, L.Z. Linan, L.H.I. Mei, Cellulose nanocrystals-based materials as hemostatic agents for wound dressings: a review, *Biomed Microdevices.* 23 (2021) 43. <https://doi.org/10.1007/s10544-021-00581-0>.
- [59] S. Homaeigohar, T.-Y. Tsai, E.S. Zarie, M. Elbahri, T.-H. Young, A.R. Boccaccini, Bovine Serum Albumin (BSA)/polyacrylonitrile (PAN) biohybrid nanofibers coated with a biomineralized calcium deficient hydroxyapatite (HA)

- shell for wound dressing, *Materials Science and Engineering: C*. 116 (2020) 111248. <https://doi.org/10.1016/j.msec.2020.111248>.
- [60] K.P. Menard, *Dynamic mechanical analysis : a practical introduction*, CRC Press, 1999.
- [61] M. Hdidar, S. Chouikhi, A. Fattoum, M. Arous, Effect of hydrolysis degree and mass molecular weight on the structure and properties of PVA films, *Ionics (Kiel)*. 23 (2017) 3125–3135. <https://doi.org/10.1007/s11581-017-2103-0>.
- [62] T.M.C. Maria, R.A. de Carvalho, P.J.A. Sobral, A.M.B.Q. Habitante, J. Solorza-Feria, The effect of the degree of hydrolysis of the PVA and the plasticizer concentration on the color, opacity, and thermal and mechanical properties of films based on PVA and gelatin blends, *J Food Eng.* 87 (2008) 191–199. <https://doi.org/10.1016/j.jfoodeng.2007.11.026>.
- [63] L.M. Gradinaru, M. Bercea, S. Vlad, M. Barbalata Mandru, M. Drobeta, M. Aflori, R.C. Ciobanu, Preparation and characterization of electrospun magnetic poly(ether urethane) nanocomposite mats: Relationships between the viscosity of the polymer solutions and the electrospinning ability, *Polymer (Guildf)*. 256 (2022) 125186. <https://doi.org/10.1016/j.polymer.2022.125186>.
- [64] X. Ma, X. Sun, D. Hargrove, J. Chen, D. Song, Q. Dong, X. Lu, T.-H. Fan, Y. Fu, Y. Lei, A Biocompatible and Biodegradable Protein Hydrogel with Green and Red Autofluorescence: Preparation, Characterization and In Vivo Biodegradation Tracking and Modeling, *Sci Rep.* 6 (2016) 19370. <https://doi.org/10.1038/srep19370>.
- [65] V. Christen, S. Faltermann, N.R. Brun, P.Y. Kunz, K. Fent, Cytotoxicity and molecular effects of biocidal disinfectants (quaternary ammonia, glutaraldehyde, poly(hexamethylene biguanide) hydrochloride PHMB) and their mixtures in vitro and in zebrafish eleuthero-embryos, *Science of The Total Environment*. 586 (2017) 1204–1218. <https://doi.org/10.1016/j.scitotenv.2017.02.114>.
- [66] D.L.S. Scheffel, D.G. Soares, F.G. Basso, C.A. de Souza Costa, D. Pashley, J. Hebling, Transdental cytotoxicity of glutaraldehyde on odontoblast-like cells, *J Dent.* 43 (2015) 997–1006. <https://doi.org/10.1016/j.jdent.2015.05.004>.
- [67] B. Zhu, W. Li, N. Chi, R. v. Lewis, J. Osamor, R. Wang, Optimization of Glutaraldehyde Vapor Treatment for Electrospun Collagen/Silk Tissue Engineering Scaffolds, *ACS Omega*. 2 (2017) 2439–2450. <https://doi.org/10.1021/acsomega.7b00290>.
- [68] G. Yang, Z. Xiao, H. Long, K. Ma, J. Zhang, X. Ren, J. Zhang, Assessment of the characteristics and biocompatibility of gelatin sponge scaffolds prepared by various crosslinking methods, *Sci Rep.* 8 (2018) 1616. <https://doi.org/10.1038/s41598-018-20006-y>.
- [69] J.T. Aladejana, Z. Wu, D. Li, K. Guelifack, W. Wei, X.A. Wang, Y. Xie, Facile Approach for Glutaraldehyde Cross-Linking of PVA/Aluminophosphate Adhesives for Wood-Based Panels, *ACS Sustain Chem Eng.* 7 (2019) 18524–18533. <https://doi.org/10.1021/acssuschemeng.9b04555>.

- [70] R. v. Gadhave, P.A. Mahanwar, P.T. Gadekar, Effect of glutaraldehyde on thermal and mechanical properties of starch and polyvinyl alcohol blends, *Des Monomers Polym.* 22 (2019) 164–170. <https://doi.org/10.1080/15685551.2019.1678222>.
- [71] R. Rudra, V. Kumar, P.P. Kundu, Acid catalysed cross-linking of poly vinyl alcohol (PVA) by glutaraldehyde: effect of crosslink density on the characteristics of PVA membranes used in single chambered microbial fuel cells, *RSC Adv.* 5 (2015) 83436–83447. <https://doi.org/10.1039/C5RA16068E>.
- [72] A.G. Destaye, C. Lin, C. Lee, Glutaraldehyde Vapor Cross-linked Nanofibrous PVA Mat with in Situ Formed Silver Nanoparticles, *ACS Appl Mater Interfaces.* (2013).
- [73] G. Tillet, B. Boutevin, B. Ameduri, Chemical reactions of polymer crosslinking and post-crosslinking at room and medium temperature, *Prog Polym Sci.* 36 (2011) 191–217. <https://doi.org/10.1016/j.progpolymsci.2010.08.003>.
- [74] W. Li, T. Li, G. Li, L. An, F. Li, Z. Zhang, Electrospun H<sub>4</sub>SiW<sub>12</sub>O<sub>40</sub>/cellulose acetate composite nanofibrous membrane for photocatalytic degradation of tetracycline and methyl orange with different mechanism, *Carbohydr Polym.* 168 (2017) 153–162. <https://doi.org/10.1016/j.carbpol.2017.03.079>.
- [75] N. Liao, A. Rajan, M. Kumar, A. Prasad, S. Tshool, C. Park, C. Sang, Electrospun bioactive poly (E -caprolactone) – cellulose acetate – dextran antibacterial composite mats for wound dressing applications, *Colloids Surf A Physicochem Eng Asp.* 469 (2015) 194–201. <https://doi.org/10.1016/j.colsurfa.2015.01.022>.
- [76] H. Liao, R. Qi, M. Shen, X. Cao, R. Guo, Y. Zhang, X. Shi, Improved cellular response on multiwalled carbon nanotube-incorporated electrospun polyvinyl alcohol/chitosan nanofibrous scaffolds, *Colloids Surf B Biointerfaces.* 84 (2011) 528–535. <https://doi.org/10.1016/j.colsurfb.2011.02.010>.
- [77] P. Vashisth, V. Pruthi, Synthesis and characterization of crosslinked gellan/PVA nanofibers for tissue engineering application, *Materials Science and Engineering C.* 67 (2016) 304–312. <https://doi.org/10.1016/j.msec.2016.05.049>.
- [78] L.M. Gradinaru, M. Bercea, S. Vlad, M. Barbalata Mandru, M. Drobot, M. Aflori, R.C. Ciobanu, Preparation and characterization of electrospun magnetic poly(ether urethane) nanocomposite mats: Relationships between the viscosity of the polymer solutions and the electrospinning ability, *Polymer (Guildf).* 256 (2022) 125186. <https://doi.org/10.1016/j.polymer.2022.125186>.
- [79] A. Mehrdad, M.T. Taghizadeh, R. Moladoust, Thermodynamic Study of Poly(ethylene glycol) in Water/1-Propanol Solutions by Viscometry, *J Solution Chem.* 40 (2011) 832–842. <https://doi.org/10.1007/s10953-011-9683-5>.
- [80] C.J. Luo, E. Stride, M. Edirisinghe, Mapping the Influence of Solubility and Dielectric Constant on Electrospinning Polycaprolactone Solutions, *Macromolecules.* 45 (2012) 4669–4680. <https://doi.org/10.1021/ma300656u>.
- [81] S. Higashi, T. Hirai, M. Matsubara, H. Yoshida, A. Beniya, Dynamic viscosity recovery of electrospinning solution for stabilizing elongated ultrafine polymer

- nanofiber by TEMPO-CNF, *Sci Rep.* 10 (2020) 13427. <https://doi.org/10.1038/s41598-020-69136-2>.
- [82] M.M. Mahmud, A. Perveen, M.A. Matin, M.T. Arafat, Effects of binary solvent mixtures on the electrospinning behavior of poly (vinyl alcohol), *Mater Res Express.* 5 (2018) 115407. <https://doi.org/10.1088/2053-1591/aadflf>.
- [83] M. Mohsen-Nia, H. Amiri, Measurement and modelling of static dielectric constants of aqueous solutions of methanol, ethanol and acetic acid at T=293.15K and 91.3kPa, *J Chem Thermodyn.* 57 (2013) 67–70. <https://doi.org/10.1016/j.jct.2012.08.009>.
- [84] A.C. Dimian, C.S. Bildea, A.A. Kiss, Acetic Acid, in: *Applications in Design and Simulation of Sustainable Chemical Processes*, Elsevier, 2019: pp. 483–519. <https://doi.org/10.1016/B978-0-444-63876-2.00013-9>.
- [85] Factors Affecting Nanofiber Quality, in: *Science and Technology of Polymer Nanofibers*, John Wiley & Sons, Inc., Hoboken, NJ, USA, n.d.: pp. 81–110. <https://doi.org/10.1002/9780470229842.ch4>.
- [86] F. Yeganeh, R. Behrooz, M. Rahimi, The effect of Sulfuric acid and Maleic acid on characteristics of nano-cellulose produced from waste office paper, *International Journal of Nano Dimension.* 8 (2017) 206–215.
- [87] P.M. Silva, C. Prieto, J.M. Lagarón, L.M. Pastrana, M.A. Coimbra, A.A. Vicente, M.A. Cerqueira, Food-grade hydroxypropyl methylcellulose-based formulations for electrohydrodynamic processing: Part I – Role of solution parameters on fibre and particle production, *Food Hydrocoll.* 118 (2021). <https://doi.org/10.1016/j.foodhyd.2021.106761>.
- [88] I.E. Moreno-Cortez, J. Romero-García, V. González-González, D.I. García-Gutierrez, M.A. Garza-Navarro, R. Cruz-Silva, Encapsulation and immobilization of papain in electrospun nanofibrous membranes of PVA cross-linked with glutaraldehyde vapor, *Materials Science and Engineering C.* 52 (2015) 306–314. <https://doi.org/10.1016/j.msec.2015.03.049>.
- [89] L. Chen, Z. Liu, J. Shi, C. Wang, L. Ding, X. Ding, G. Teng, J. Wu, J. Zhang, Preparation and antibacterial properties of chitosan/polyvinyl alcohol nanofibrous mats using different organic acids as solvents, *Process Biochemistry.* 122 (2022) 13–28. <https://doi.org/10.1016/j.procbio.2022.08.025>.
- [90] I. Negut, G. Dorcioman, V. Grumezescu, Scaffolds for Wound Healing Applications, *Polymers (Basel).* 12 (2020) 2010. <https://doi.org/10.3390/polym12092010>.
- [91] M. Abrigo, S.L. McArthur, P. Kingshott, Electrospun Nanofibers as Dressings for Chronic Wound Care: Advances, Challenges, and Future Prospects, *Macromol Biosci.* 14 (2014) 772–792. <https://doi.org/10.1002/mabi.201300561>.
- [92] S. Fahimirad, F. Ajalloueiian, Naturally-derived electrospun wound dressings for target delivery of bio-active agents, *Int J Pharm.* 566 (2019) 307–328. <https://doi.org/10.1016/j.ijpharm.2019.05.053>.

- [93] J. Yin, L. Xu, Batch preparation of electrospun polycaprolactone/chitosan/aloe vera blended nanofiber membranes for novel wound dressing, *Int J Biol Macromol.* 160 (2020) 352–363. <https://doi.org/10.1016/j.ijbiomac.2020.05.211>.
- [94] Y. Liang, Y. Liang, H. Zhang, B. Guo, Antibacterial biomaterials for skin wound dressing, *Asian J Pharm Sci.* 17 (2022) 353–384. <https://doi.org/10.1016/j.ajps.2022.01.001>.
- [95] M.A. Teixeira, J.C. Antunes, C.L. Seabra, A. Fertuzinhos, S.D. Tohidi, S. Reis, M.T.P. Amorim, D.P. Ferreira, H.P. Felgueiras, Antibacterial and hemostatic capacities of cellulose nanocrystalline-reinforced poly(vinyl alcohol) electrospun mats doped with Tiger 17 and pexiganan peptides for prospective wound healing applications, *Biomaterials Advances.* 137 (2022) 212830. <https://doi.org/10.1016/j.bioadv.2022.212830>.
- [96] R. Xu, H. Xia, W. He, Z. Li, J. Zhao, B. Liu, Y. Wang, Q. Lei, Y. Kong, Y. Bai, Z. Yao, R. Yan, H. Li, R. Zhan, S. Yang, G. Luo, J. Wu, Controlled water vapor transmission rate promotes wound-healing via wound re-epithelialization and contraction enhancement, *Sci Rep.* 6 (2016) 24596. <https://doi.org/10.1038/srep24596>.
- [97] P.A. Vinodhini, S. K., G. Thandapani, S. P.N., V. Jayachandran, A. Sukumaran, FTIR, XRD and DSC studies of nanochitosan, cellulose acetate and polyethylene glycol blend ultrafiltration membranes, *Int J Biol Macromol.* 104 (2017) 1721–1729. <https://doi.org/10.1016/j.ijbiomac.2017.03.122>.
- [98] W. Chen, J. Ding, X. Yan, W. Yan, M. He, G. Yin, Plasticization of Cottonseed Protein/Polyvinyl Alcohol Blend Films, *Polymers (Basel).* 11 (2019) 2096. <https://doi.org/10.3390/polym11122096>.
- [99] S. Gupta, A.K. Pramanik, A. Kailath, T. Mishra, A. Guha, S. Nayar, A. Sinha, Composition dependent structural modulations in transparent poly(vinyl alcohol) hydrogels, *Colloids Surf B Biointerfaces.* 74 (2009) 186–190. <https://doi.org/10.1016/j.colsurfb.2009.07.015>.
- [100] M.S. Islam, A.N. Naz, M.N. Alam, A.K. Das, J.H. Yeum, Electrospun poly(vinyl alcohol)/silver nanoparticle/carbon nanotube multi-composite nanofiber mat: Fabrication, characterization and evaluation of thermal, mechanical and antibacterial properties, *Colloid Interface Sci Commun.* 35 (2020) 100247. <https://doi.org/10.1016/j.colcom.2020.100247>.
- [101] Md.S. Islam, J.H. Yeum, Electrospun pullulan/poly(vinyl alcohol)/silver hybrid nanofibers: Preparation and property characterization for antibacterial activity, *Colloids Surf A Physicochem Eng Asp.* 436 (2013) 279–286. <https://doi.org/10.1016/j.colsurfa.2013.07.001>.
- [102] A. Rojas, E. Velásquez, L. Garrido, M.J. Galotto, C. López de Dicastillo, Design of active electrospun mats with single and core-shell structures to achieve different curcumin release kinetics, *J Food Eng.* 273 (2020) 109900. <https://doi.org/10.1016/j.jfoodeng.2019.109900>.
- [103] M.S. Peresin, Y. Habibi, J.O. Zoppe, J.J. Pawlak, O.J. Rojas, Nanofiber Composites of Polyvinyl Alcohol and Cellulose Nanocrystals: Manufacture and

- Characterization, *Biomacromolecules*. 11 (2010) 674–681. <https://doi.org/10.1021/bm901254n>.
- [104] C.-Y. Huang, K.-H. Hu, Z.-H. Wei, Comparison of cell behavior on pva/pva-gelatin electrospun nanofibers with random and aligned configuration, *Sci Rep*. 6 (2016) 37960. <https://doi.org/10.1038/srep37960>.
- [105] E. Rynkowska, K. Fatyeyeva, S. Marais, J. Kujawa, W. Kujawski, Chemically and thermally crosslinked PVA-based membranes: Effect on swelling and transport behavior, *Polymers (Basel)*. 11 (2019). <https://doi.org/10.3390/polym11111799>.
- [106] Y. Park, M. You, J. Shin, S. Ha, D. Kim, M.H. Heo, J. Nah, Y.A. Kim, J.H. Seol, Thermal conductivity enhancement in electrospun poly(vinyl alcohol) and poly(vinyl alcohol)/cellulose nanocrystal composite nanofibers, *Sci Rep*. 9 (2019) 3026. <https://doi.org/10.1038/s41598-019-39825-8>.
- [107] J. Prakash, K.S. Venkataprasanna, G. Bharath, F. Banat, R. Niranjana, G.D. Venkatasubbu, In-vitro evaluation of electrospun cellulose acetate nanofiber containing Graphene oxide/TiO<sub>2</sub>/Curcumin for wound healing application, *Colloids Surf A Physicochem Eng Asp*. 627 (2021) 127166. <https://doi.org/10.1016/j.colsurfa.2021.127166>.
- [108] W. Wan Ishak, I. Ahmad, S. Ramli, M. Mohd Amin, Gamma Irradiation-Assisted Synthesis of Cellulose Nanocrystal-Reinforced Gelatin Hydrogels, *Nanomaterials*. 8 (2018) 749. <https://doi.org/10.3390/nano8100749>.
- [109] J. Gong, J. Li, J. Xu, Z. Xiang, L. Mo, Research on cellulose nanocrystals produced from cellulose sources with various polymorphs, *RSC Adv*. 7 (2017) 33486–33493. <https://doi.org/10.1039/C7RA06222B>.
- [110] M. Thakur, A. Sharma, V. Ahlawat, M. Bhattacharya, S. Goswami, Process optimization for the production of cellulose nanocrystals from rice straw derived  $\alpha$ -cellulose, *Mater Sci Energy Technol*. 3 (2020) 328–334. <https://doi.org/10.1016/j.mset.2019.12.005>.
- [111] Y. Li, S. Yao, High stability under extreme condition of the poly(vinyl alcohol) nanofibers crosslinked by glutaraldehyde in organic medium, *Polym Degrad Stab*. 137 (2017) 229–237. <https://doi.org/10.1016/j.polymdegradstab.2017.01.018>.
- [112] M. Ferrández-Rives, Á. Beltrán-Osuna, J. Gómez-Tejedor, J. Gómez Ribelles, Electrospun PVA/Bentonite Nanocomposites Mats for Drug Delivery, *Materials*. 10 (2017) 1448. <https://doi.org/10.3390/ma10121448>.
- [113] Z. Khatri, K. Wei, B.S. Kim, I.S. Kim, Effect of deacetylation on wicking behavior of co-electrospun cellulose acetate/polyvinyl alcohol nanofibers blend, *Carbohydr Polym*. 87 (2012) 2183–2188. <https://doi.org/10.1016/j.carbpol.2011.10.046>.
- [114] Fixation for Electron Microscopy, Elsevier, 1981. <https://doi.org/10.1016/B978-0-12-333920-1.X5001-0>.
- [115] M.S. Peresin, Y. Habibi, J.O. Zoppe, J.J. Pawlak, O.J. Rojas, Nanofiber Composites of Polyvinyl Alcohol and Cellulose Nanocrystals: Manufacture and Characterization, *Biomacromolecules*. 11 (2010) 674–681. <https://doi.org/10.1021/bm901254n>.



- [116] J.-C. Park, T. Ito, K.-O. Kim, K.-W. Kim, B.-S. Kim, M.-S. Khil, H.-Y. Kim, I.-S. Kim, Electrospun poly(vinyl alcohol) nanofibers: effects of degree of hydrolysis and enhanced water stability, *Polym J.* 42 (2010) 273–276. <https://doi.org/10.1038/pj.2009.340>.
- [117] M.S. Enayati, R. Esmaeely Neisiany, P. Sajkiewicz, T. Behzad, P. Denis, F. Pierini, Effect of nanofiller incorporation on thermomechanical and toughness of poly (vinyl alcohol)-based electrospun nanofibrous bionanocomposites, *Theoretical and Applied Fracture Mechanics.* 99 (2019) 44–50. <https://doi.org/10.1016/j.tafmec.2018.11.006>.
- [118] Y. Park, M. You, J. Shin, S. Ha, D. Kim, M.H. Heo, J. Nah, Y.A. Kim, J.H. Seol, Thermal conductivity enhancement in electrospun poly(vinyl alcohol) and poly(vinyl alcohol)/cellulose nanocrystal composite nanofibers, *Sci Rep.* 9 (2019) 1–10. <https://doi.org/10.1038/s41598-019-39825-8>.
- [119] M. Popescu, B. Dogaru, M. Goanta, D. Timpu, Structural and morphological evaluation of CNC reinforced PVA / Starch biodegradable films, *Int J Biol Macromol.* 116 (2018) 385–393. <https://doi.org/10.1016/j.ijbiomac.2018.05.036>.
- [120] E. Jin, J. Guo, F. Yang, Y. Zhu, J. Song, Y. Jin, O.J. Rojas, On the polymorphic and morphological changes of cellulose nanocrystals (CNC-I) upon mercerization and conversion to CNC-II, *Carbohydr Polym.* 143 (2016) 327–335. <https://doi.org/10.1016/j.carbpol.2016.01.048>.
- [121] N. Pandi, S.H. Sonawane, K.A. Kishore, Ultrasonics - Sonochemistry Synthesis of cellulose nanocrystals ( CNCs ) from cotton using ultrasound- assisted acid hydrolysis, *Ultrason Sonochem.* 70 (2021) 105353. <https://doi.org/10.1016/j.ultsonch.2020.105353>.
- [122] Q. Zhang, Q. Li, L. Zhang, S. Wang, D.P. Harper, Q. Wu, T.M. Young, Preparation of electrospun nanofibrous poly(vinyl alcohol)/cellulose nanocrystals air filter for efficient particulate matter removal with repetitive usage capability via facile heat treatment, *Chemical Engineering Journal.* 399 (2020) 125768. <https://doi.org/10.1016/j.cej.2020.125768>.
- [123] Y. Park, M. You, J. Shin, S. Ha, D. Kim, M.H. Heo, J. Nah, Y.A. Kim, J.H. Seol, Thermal conductivity enhancement in electrospun poly(vinyl alcohol) and poly(vinyl alcohol)/cellulose nanocrystal composite nanofibers, *Sci Rep.* 9 (2019) 3026. <https://doi.org/10.1038/s41598-019-39825-8>.
- [124] M.S. Enayati, R. Esmaeely Neisiany, P. Sajkiewicz, T. Behzad, P. Denis, F. Pierini, Effect of nanofiller incorporation on thermomechanical and toughness of poly (vinyl alcohol)-based electrospun nanofibrous bionanocomposites, *Theoretical and Applied Fracture Mechanics.* 99 (2019) 44–50. <https://doi.org/10.1016/j.tafmec.2018.11.006>.
- [125] S.M. Lemma, M. Scampicchio, P.J. Mahon, I. Sbarski, J. Wang, P. Kingshott, Controlled Release of Retinyl Acetate from  $\beta$ -Cyclodextrin Functionalized Poly(vinyl alcohol) Electrospun Nanofibers, *J Agric Food Chem.* 63 (2015) 3481–3488. <https://doi.org/10.1021/acs.jafc.5b00103>.

- [126] U. Khan, K. Ryan, W.J. Blau, J.N. Coleman, The effect of solvent choice on the mechanical properties of carbon nanotube–polymer composites, *Compos Sci Technol.* 67 (2007) 3158–3167. <https://doi.org/10.1016/j.compscitech.2007.04.015>.
- [127] J.-C. Park, T. Ito, K.-O. Kim, K.-W. Kim, B.-S. Kim, M.-S. Khil, H.-Y. Kim, I.-S. Kim, Electrospun poly(vinyl alcohol) nanofibers: effects of degree of hydrolysis and enhanced water stability, *Polym J.* 42 (2010) 273–276. <https://doi.org/10.1038/pj.2009.340>.
- [128] A. Mohamed, V.L.F. Finkenstadt, S.H.G. Gordon, G. Biresaw, P. E., Debra, P. Rayas-Duarte, Thermal Properties of PCL/Gluten Bioblends Characterized by TGA, DSC, SEM, and Infrared-PAS, *J Appl Polym Sci.* 116 (2010) 2658–2667. <https://doi.org/10.1002/app>.
- [129] S.N. Cassu, M.I. Felisberti, Poly(vinyl alcohol) and poly(vinylpyrrolidone) blends: 2. Study of relaxations by dynamic mechanical analysis, *Polymer (Guildf)*. 40 (1999) 4845–4851. [https://doi.org/10.1016/S0032-3861\(98\)00703-4](https://doi.org/10.1016/S0032-3861(98)00703-4).
- [130] W. Yang, X. He, F. Luzi, W. Dong, T. Zheng, J.M. Kenny, D. Puglia, P. Ma, Thermomechanical, antioxidant and moisture behaviour of PVA films in presence of citric acid esterified cellulose nanocrystals, *Int J Biol Macromol.* 161 (2020) 617–626. <https://doi.org/10.1016/j.ijbiomac.2020.06.082>.
- [131] A.E. Amooghini, M.Z. Pedram, M. Omidkhah, R. Yegani, A novel CO<sub>2</sub>-selective synthesized amine-impregnated cross-linked polyvinylalcohol/glutaraldehyde membrane: fabrication, characterization, and gas permeation study, *Greenhouse Gases: Science and Technology.* 3 (2013) 378–391. <https://doi.org/10.1002/ghg.1369>.
- [132] P.A. Vinodhini, S. K., G. Thandapani, S. P.N., V. Jayachandran, A. Sukumaran, FTIR, XRD and DSC studies of nanochitosan, cellulose acetate and polyethylene glycol blend ultrafiltration membranes, *Int J Biol Macromol.* 104 (2017) 1721–1729. <https://doi.org/10.1016/j.ijbiomac.2017.03.122>.
- [133] D. Salamon, *Advanced Ceramics*, in: *Advanced Ceramics for Dentistry*, Elsevier, 2014: pp. 103–122. <https://doi.org/10.1016/B978-0-12-394619-5.00006-7>.
- [134] H. Adeli, M.T. Khorasani, M. Parvazinia, Wound dressing based on electrospun PVA/chitosan/starch nanofibrous mats: Fabrication, antibacterial and cytocompatibility evaluation and in vitro healing assay, *Int J Biol Macromol.* 122 (2019) 238–254. <https://doi.org/10.1016/j.ijbiomac.2018.10.115>.
- [135] L.A. Can-Herrera, A.I. Oliva, M.A.A. Dzul-Cervantes, O.F. Pacheco-Salazar, J.M. Cervantes-Uc, Morphological and Mechanical Properties of Electrospun Polycaprolactone Scaffolds: Effect of Applied Voltage, *Polymers (Basel)*. 13 (2021) 662. <https://doi.org/10.3390/polym13040662>.
- [136] U. Stachewicz, R.J. Bailey, W. Wang, A.H. Barber, Size dependent mechanical properties of electrospun polymer fibers from a composite structure, *Polymer (Guildf)*. 53 (2012) 5132–5137. <https://doi.org/10.1016/j.polymer.2012.08.064>.

- [137] T.U. Rashid, R.E. Gorga, W.E. Krause, Mechanical Properties of Electrospun Fibers—A Critical Review, *Adv Eng Mater.* 23 (2021) 2100153. <https://doi.org/10.1002/adem.202100153>.
- [138] S. Choy, H. Moon, Y. Park, Y.M. Jung, J.M. Koo, D.X. Oh, D.S. Hwang, Mechanical properties and thermal stability of intermolecular-fitted poly(vinyl alcohol)/ $\alpha$ -chitin nanofibrous mat, *Carbohydr Polym.* 244 (2020). <https://doi.org/10.1016/j.carbpol.2020.116476>.
- [139] N. Jain, V.K. Singh, S. Chauhan, Dynamic and creep analysis of polyvinyl alcohol based films blended with starch and protein, *Journal of Polymer Engineering.* 39 (2019) 35–47. <https://doi.org/10.1515/polyeng-2018-0032>.
- [140] J.E. Sanders, Y. Han, T.S. Rushing, D.J. Gardner, Electrospinning of Cellulose Nanocrystal-Filled Poly (Vinyl Alcohol) Solutions: Material Property Assessment, *Nanomaterials.* 9 (2019) 805. <https://doi.org/10.3390/nano9050805>.
- [141] J. Chen, H. Yang, J. Li, J. Chen, Y. Zhang, X. Zeng, The development of an artificial skin model and its frictional interaction with wound dressings, *J Mech Behav Biomed Mater.* 94 (2019) 308–316. <https://doi.org/10.1016/j.jmbbm.2019.03.013>.
- [142] W.J. Lee, A.J. Clancy, E. Kontturi, A. Bismarck, M.S.P. Shaffer, Strong and Stiff: High-Performance Cellulose Nanocrystal/Poly(vinyl alcohol) Composite Fibers, *ACS Appl Mater Interfaces.* 8 (2016) 31500–31504. <https://doi.org/10.1021/acsami.6b11578>.
- [143] S.M. Costa, D.P. Ferreira, P. Teixeira, L.F. Ballesteros, J.A. Teixeira, R. Figueiro, Active natural-based films for food packaging applications: The combined effect of chitosan and nanocellulose, *Int J Biol Macromol.* 177 (2021) 241–251. <https://doi.org/10.1016/j.ijbiomac.2021.02.105>.
- [144] J.E. Sanders, Y. Han, T.S. Rushing, D.J. Gardner, Electrospinning of Cellulose Nanocrystal-Filled Poly (Vinyl Alcohol) Solutions: Material Property Assessment, *Nanomaterials.* 9 (2019) 805. <https://doi.org/10.3390/nano9050805>.
- [145] C. Zhou, R. Chu, R. Wu, Q. Wu, Electrospun Polyethylene Oxide/Cellulose Nanocrystal Composite Nanofibrous Mats with Homogeneous and Heterogeneous Microstructures, *Biomacromolecules.* 12 (2011) 2617–2625. <https://doi.org/10.1021/bm200401p>.
- [146] V. Favier, H. Chanzy, J.Y. Cavaille, Polymer Nanocomposites Reinforced by Cellulose Whiskers, *Macromolecules.* 28 (1995) 6365–6367. <https://doi.org/10.1021/ma00122a053>.
- [147] F. Ansari, M. Salajková, Q. Zhou, L.A. Berglund, Strong Surface Treatment Effects on Reinforcement Efficiency in Biocomposites Based on Cellulose Nanocrystals in Poly(vinyl acetate) Matrix, *Biomacromolecules.* 16 (2015) 3916–3924. <https://doi.org/10.1021/acs.biomac.5b01245>.
- [148] V.-T. Pham, T.-H. Fang, Thermal and mechanical characterization of nanoporous two-dimensional MoS<sub>2</sub> membranes, *Sci Rep.* 12 (2022) 7777. <https://doi.org/10.1038/s41598-022-11883-5>.

- [149] S. Ahmed, C. Wei-, Preparation of Antibacterial Electrospun PVA / Regenerated Silk Fibroin Nanofibrous Composite Containing Ciprofloxacin Hydrochloride as a Wound Dressing, (2014).
- [150] O.A.C. Monteiro, C. Airoidi, Some studies of crosslinking chitosan–glutaraldehyde interaction in a homogeneous system, *Int J Biol Macromol.* 26 (1999) 119–128. [https://doi.org/10.1016/S0141-8130\(99\)00068-9](https://doi.org/10.1016/S0141-8130(99)00068-9).
- [151] S. Khorshidi, A. Solouk, A. Karkhaneh, H. Mirzadeh, S. Sharifi, S. Mazinani, Effect of crosslinking procedure on structural, thermal, and functional performances of cellulosic nanofibers: A comparison between chemical and photochemical crosslinking, *J Appl Polym Sci.* 133 (2016). <https://doi.org/10.1002/app.43832>.
- [152] L. Jiang, K. Li, H. Yang, X. Liu, W. Li, W. Xu, B. Deng, Improving mechanical properties of electrospun cellulose acetate nanofiber membranes by cellulose nanocrystals with and without polyvinylpyrrolidone, *Cellulose.* 27 (2020) 955–967. <https://doi.org/10.1007/s10570-019-02830-1>.
- [153] K.A. Sindhu, R. Prasanth, V. Kumar, *Medical Applications of Cellulose and Its Derivatives : Present and Future*, 2015.
- [154] H. Huang, D. Dean, 3-D printed porous cellulose acetate tissue scaffolds for additive manufacturing, *Addit Manuf.* 31 (2020) 100927. <https://doi.org/10.1016/j.addma.2019.100927>.
- [155] *Bioinspired and Biomimetic Materials for Drug Delivery*, Elsevier, 2021. <https://doi.org/10.1016/C2019-0-02454-5>.
- [156] Z. Cui, Z. Zheng, L. Lin, J. Si, Q. Wang, X. Peng, W. Chen, Electrospinning and crosslinking of polyvinyl alcohol/chitosan composite nanofiber for transdermal drug delivery, *Advances in Polymer Technology.* 37 (2018) 1917–1928. <https://doi.org/10.1002/adv.21850>.
- [157] J.M. Yang, J.H. Yang, S.C. Tsou, C.H. Ding, C.C. Hsu, K.C. Yang, C.C. Yang, K.S. Chen, S.W. Chen, J.S. Wang, Cell proliferation on PVA/sodium alginate and PVA/poly( $\gamma$ -glutamic acid) electrospun fiber, *Materials Science and Engineering C.* 66 (2016) 170–177. <https://doi.org/10.1016/j.msec.2016.04.068>.
- [158] J.H. Park, G.C. Rutledge, Ultrafine high performance polyethylene fibers, *J Mater Sci.* 53 (2018) 3049–3063. <https://doi.org/10.1007/s10853-017-1724-z>.
- [159] A.S. Rojas-Mercado, I.E. Moreno-Cortez, R. Lucio-Porto, L.L. Pavón, Encapsulation and immobilization of ficin extract in electrospun polymeric nanofibers, *Int J Biol Macromol.* 118 (2018) 2287–2295. <https://doi.org/10.1016/j.ijbiomac.2018.07.113>.

**Highlights**

- PVA/CA and PVA/CNC miscibility was confirmed by TGA and DSC assessments.
- Upon addition of CA and CNC to PVA, the mats' thermal capacity was increased.
- Crosslinking augmented the nanofibers' diameters but reduced their crystallinity.
- CA and CNC doped mats displayed a superior Young's modulus.
- E' evidenced the strength of the physical interactions between polymers.

**Declaration of interests**

The authors declare that they have no known competing financial interests or personal relationships that could have appeared to influence the work reported in this paper.

The authors declare the following financial interests/personal relationships which may be considered as potential competing interests:

Journal Pre-proof